

Tensor parametric Hamiltonian operator inference

Arjun Vijaywargiya^{1,2}, Shane A. McQuarrie³, and Anthony Gruber^{*2}

¹*Department of Applied and Computational Mathematics and Statistics, University of Notre Dame*

²*Computational Mathematics, Center for Computing Research, Sandia National Laboratories*

³*Scientific Machine Learning, Center for Computing Research, Sandia National Laboratories*

Abstract

This work presents a tensor-based approach to constructing data-driven reduced-order models corresponding to semi-discrete partial differential equations with canonical Hamiltonian structure. By expressing parameter-varying operators with affine dependence as contractions of a generalized parameter vector against a constant tensor, this method leverages the operator inference framework to capture parametric dependence in the learned reduced-order model via the solution to a convex, least-squares optimization problem. This leads to a concise and straightforward implementation which compactifies previous parametric operator inference approaches and directly extends to learning parametric operators with symmetry constraints—a key feature required for constructing structure-preserving surrogates of Hamiltonian systems. The proposed approach is demonstrated on both a (non-Hamiltonian) heat equation with variable diffusion coefficient as well as a Hamiltonian wave equation with variable wave speed.

Keywords: parametric model reduction, tensor calculus, Hamiltonian systems, structure preservation, scientific machine learning

1 Introduction

Mathematical models based on partial differential equations (PDEs) are often formed through the combination of terms describing locally distinct physical processes. For example, an advection-diffusion equation describing the evolution of a scalar quantity q on a domain $\Omega \subset \mathbb{R}^d$, given by $\partial_t q = \nabla \cdot (\mathbf{D}\nabla q - \mathbf{v}q)$ for appropriate diffusion field \mathbf{D} and velocity \mathbf{v} , combines the term $\nabla \cdot (\mathbf{D}\nabla q)$ expressing diffusion with a corresponding term $\mathbf{v} \cdot \nabla q$ describing material transport. The practical utility of PDE-based models typically relies on the calibration of a number of parameters (\mathbf{D}, \mathbf{v} in the example above), which are critical to the behavior of solutions, hence also to the physical realism of the relevant model. Moreover, these parameters are manifestly application dependent, meaning that any sufficiently general technique for constructing data-driven surrogate models for physical systems must be amenable to parametric variability. This paper develops a data-driven method of constructing reduced-order models (ROMs)—low-dimensional dynamical systems for approximating the dominant dynamics of a large-scale physical model—which seamlessly encoding parametric dependencies while simultaneously preserving other structural features of interest.

The development of parametric ROMs is straightforward and well understood in the case of intrusive, projection-based methods [3, 4, 19, 38, 50, 51]. Given a numerical simulator—termed the full-order model (FOM) due to it usually having a large number of degrees of freedom—for a physical process, intrusive methods define a ROM through Galerkin projection onto a low-dimensional manifold which, ideally, captures the dominant state behavior the system. In this setting, any parametric dependence appearing in the FOM is automatically inherited by the resulting ROM. However, intrusive methods require direct manipulation of the FOM equations as well as access to the underlying operators in the FOM source code. This may not always be possible, for instance when using proprietary or complex legacy codes whose implementations are inaccessible or not amenable to modifications. Even when codes are available, the direct manipulations required by intrusive model reduction can be highly non-trivial and error prone.

*Corresponding author. E-mail: adgrube@sandia.gov.

In response to these challenges, many non-intrusive model reduction strategies have recently been developed and successfully applied to a variety of large-scale systems. In contrast to generating ROM equations through the direct projection of FOM equations, non-intrusive model reduction techniques typically rely on the use of a pre-specified model form, along with snapshot data of FOM solutions, to infer a ROM which can be simulated without access to FOM code. Several approaches, including as dynamic mode decomposition (DMD) [41, 42] and operator inference (OpInf) [17, 30, 35], define a convex linear least-squares regression to infer ROM components. In their standard (non-parametric) forms, these approaches tend to “average out” the effects of parameter dependence. To better accommodate parametric problems, extensions have been developed to DMD [9, 26, 39] and OpInf [33, 53] that build known parametric structure into the pre-specified model form. Other strategies use more general regression techniques, such as Gaussian process regression [23, 24] or deep learning [7, 11, 12].

An additional challenge in model reduction generally—and one that can be especially detrimental to data-driven methods in particular if left unaddressed—is to ensure that a ROM possesses certain desired properties of the dynamics being approximated. For instance, this paper focuses on (canonical) Hamiltonian systems, which feature a symplectic structure and conserve the total energy of solutions [31]. Several strategies exist to guarantee such properties in surrogates learned from data (see, e.g., [6, 20, 28]); in particular, the OpInf framework has enjoyed several recent extensions specifically catered to gradient flows and Hamiltonian systems [15, 16, 21, 44, 46, 47]. The OpInf formulations that impose structural constraints also tends to negate the need for regularization techniques to stabilize the dynamics of the resulting ROMs [32, 33, 37]. However, enforcing structure also tends to increase the complexity of the associated inference procedure mathematically, computationally, and in terms of the difficulty implementation. Each of these issues are further compounded by the presence of parametric variations.

The purpose of the present work is to develop a simple and general way to incorporate parametric dependence into the OpInf framework and, simultaneously, the preservation of structural properties in the resulting ROM. The following simple observation is key: when a matrix operator $\mathbf{A}(\boldsymbol{\mu}) : \mathbb{R}^N \rightarrow \mathbb{R}^N$ depends linearly on a known function $\boldsymbol{\mu}' = \boldsymbol{\theta}(\boldsymbol{\mu}) \in \mathbb{R}^{p'}$ of the parameter vector $\boldsymbol{\mu} \in \mathbb{R}^p$, then $\mathbf{A}(\boldsymbol{\mu}) = \mathbf{T}\boldsymbol{\mu}'$ can be written as the contraction of a *constant* tensor $\mathbf{T} \in \mathbb{R}^{N \times N \times p'}$ against the transformed parameters $\boldsymbol{\mu}' \in \mathbb{R}^{p'}$. Said differently, the adjoint relationship $A \mapsto (B \mapsto C) \cong (A \otimes B) \mapsto C$ between continuous linear mappings \mapsto of vector spaces and the tensor product \otimes yields a description of the “affine” parametric dependence in $\mathbf{A}(\boldsymbol{\mu})$ in terms of the linear action of a constant tensor \mathbf{T} on $\boldsymbol{\mu}'$. This notion is general enough to encompass a wide range of parametric behavior and will be shown to enable an OpInf learning problem which does not rely on local approximation techniques such as Taylor expansion [10] or linear interpolation [35]. This approach builds on previous OpInf methods for affine parametric system [33, 54] while also enabling a novel extension to parametric Hamiltonian systems, in which the preservation of certain structure information is critical to stability and predictive accuracy. The extension is natural given the mathematical concision and streamlined implementation brought about by the tensorized approach. To summarize, the contributions of this article are twofold: first, a tensor-based approach to parametric OpInf which is convex, mathematically concise, simple to implement, and recovers previous work as a special case; and second, an extension of parametric OpInf methodology to systems with Hamiltonian structure, leading to non-intrusive parametric ROMs which guarantee symplecticity and the production of conservative Hamiltonian dynamics.

The remainder of the work is structured as follows. Section 2 presents the proposed tensor parametric approach in the structure-agnostic case by defining a data-driven tensor inference problem, expressing its closed form solution, analyzing uniqueness conditions, and detailing concise numerical implementations. Section 3 discusses Hamiltonian systems and extends the tensor parametric inference to operators with symmetry appropriate for reduced-order models of Hamiltonian dynamics. Section 4 presents numerical results for parametric heat and wave equations to test the approaches of Section 2 and Section 3, respectively, demonstrating the performance of the proposed method. Finally, Section 5 offers some concluding remarks and avenues for future work.

2 Tensor parametric operator inference

This section focuses on systems of ordinary differential equations (ODEs) with affine parametric dependence but without symmetry or conservation properties. Section 2.1 defines the problem setting and introduces

tensorized forms of both the original and approximate reduced dynamics. In Section 2.2, a strategy is presented and analyzed for learning reduced tensorized parametric dynamics from state data. Section 2.3 then outlines an example where the methodology can be applied, with numerical results deferred to Section 4.

2.1 Affine parametric linear systems

Consider a linear parametric system of ODEs in which the dynamics depends affinely (i.e., generalized linearly) on a vector $\boldsymbol{\mu} \in \mathbb{R}^p$ of parameters:

$$\mathbf{M}\dot{\mathbf{q}} = \mathbf{A}(\boldsymbol{\mu})\mathbf{q}, \quad \mathbf{q}(0, \boldsymbol{\mu}) = \mathbf{q}_0(\boldsymbol{\mu}), \quad \mathbf{A}(\boldsymbol{\mu}) = \sum_{x=1}^{p'} \theta_x(\boldsymbol{\mu})\mathbf{A}_x, \quad (2.1)$$

where $\mathbf{q} = \mathbf{q}(t, \boldsymbol{\mu}) \in \mathbb{R}^N$ is the ODE state vector, $\mathbf{q}_0(\boldsymbol{\mu}) \in \mathbb{R}^N$ is a given initial condition, $\mathbf{M} \in \mathbb{R}^{N \times N}$ is symmetric positive definite (e.g., a mass matrix in a finite element method), and $\mathbf{A} : \mathbb{R}^p \rightarrow \mathbb{R}^{N \times N}$ is a matrix-valued function defined by the (possibly nonlinear) scalar-valued functions $\theta_1, \dots, \theta_{p'} : \mathbb{R}^p \rightarrow \mathbb{R}$ and constant matrices $\mathbf{A}_1, \dots, \mathbf{A}_{p'} \in \mathbb{R}^{N \times N}$. Such systems frequently arise from a method of lines semi-discretization of time-dependent PDEs (see, e.g., [52]). As the discrete dimension N is typically very large, (2.1) is called the *full-order model* (FOM), which serves as the best available discretization of the dynamics under consideration.

When the matrices $\mathbf{A}_1, \dots, \mathbf{A}_{p'}$ can be accessed intrusively, it is straightforward to construct a computationally efficient *reduced-order model* (ROM) for (2.1) through projection. This paper considers projection onto \mathbf{M} -orthonormal linear reduced bases $\mathbf{U} \in \mathbb{R}^{N \times r}$ ($r \ll N$), though nonlinear approximations such as in [2, 13, 14, 27, 43] may also be considered with minor alterations to the approach. More precisely, given a trial space basis $\mathbf{U} \in \mathbb{R}^{N \times r}$ satisfying $\mathbf{U}^\top \mathbf{M} \mathbf{U} = \mathbf{I}$ and a low-rank approximation $\hat{\mathbf{q}} := \mathbf{U} \hat{\mathbf{q}} \approx \mathbf{q}$ defined in terms of an unknown coefficient vector $\hat{\mathbf{q}} = \hat{\mathbf{q}}(t, \boldsymbol{\mu}) \in \mathbb{R}^r$, Galerkin projection of the FOM (2.1) onto the column space of \mathbf{U} gives the following reduced ODE system [3]:

$$\dot{\hat{\mathbf{q}}} = \mathbf{U}^\top \mathbf{A}(\boldsymbol{\mu}) \mathbf{U} \hat{\mathbf{q}} = \sum_{x=1}^{p'} \theta_x(\boldsymbol{\mu}) \hat{\mathbf{A}}_x \hat{\mathbf{q}}, \quad \hat{\mathbf{q}}(0, \boldsymbol{\mu}) = \mathbf{U}^\top \mathbf{M} \mathbf{q}_0(\boldsymbol{\mu}), \quad (2.2)$$

where $\hat{\mathbf{A}}_x := \mathbf{U}^\top \mathbf{A}_x \mathbf{U} \in \mathbb{R}^{r \times r}$ for each $x = 1, \dots, p'$. The system (2.2) is a low-dimensional approximation to the FOM (2.1) which, importantly, exhibits the same affine-parametric structure as the FOM. Provided the trial space basis \mathbf{U} is well chosen (e.g., L^2 -optimal over some data range), the ROM (2.2) can accurately recover the dominant behavior of the original system at a significantly reduced computational cost, since the matrices $\hat{\mathbf{A}}_1, \dots, \hat{\mathbf{A}}_{p'}$ can be pre-computed once and reused for multiple values of the parameter $\boldsymbol{\mu}$. However, computing each $\hat{\mathbf{A}}_x$ involves direct matrix-matrix multiplications with the full-order object \mathbf{A}_x , an intrusive procedure that requires access to the code implementing the FOM (2.1). The goal of parametric OpInf is to non-intrusively construct a ROM similar to (2.2) by inferring low-dimensional operators from observations of the state \mathbf{q} .

Remark 2.1 (Basis orthonormality). The reduced-order matrix $\hat{\mathbf{A}}(\boldsymbol{\mu}) = \mathbf{U}^\top \mathbf{A}(\boldsymbol{\mu}) \mathbf{U}$ is symmetric (or skew symmetric) whenever the full-order matrix $\mathbf{A}(\boldsymbol{\mu})$ is. If a basis \mathbf{U} is chosen which is not \mathbf{M} -orthonormal, Galerkin projection results in the slightly different ROM

$$\dot{\hat{\mathbf{q}}} = (\mathbf{U}^\top \mathbf{M} \mathbf{U})^{-1} \mathbf{U}^\top \mathbf{A}(\boldsymbol{\mu}) \mathbf{U} \hat{\mathbf{q}},$$

which does not inherit (anti-)symmetry from the FOM. This paper focuses on \mathbf{M} -orthonormal bases because the goal of Section 3 is to construct ROMs which preserve system symmetry without direct access to $\mathbf{A}(\boldsymbol{\mu})$.

Before proceeding, it is convenient to reformulate (2.1) and (2.2) in a way which exposes their tensorial structure. Let $\boldsymbol{\mu}' = \boldsymbol{\theta}(\boldsymbol{\mu}) := (\theta_1(\boldsymbol{\mu}), \dots, \theta_{p'}(\boldsymbol{\mu}))^\top \in \mathbb{R}^{p'}$ denote the vector of scalar coefficients in the affine expansion of $\mathbf{A}(\boldsymbol{\mu})$. Then the FOM (2.1) can be written in the compact form

$$\mathbf{M}\dot{\mathbf{q}} = (\mathbf{T}\boldsymbol{\mu}')\mathbf{q}, \quad \mathbf{q}(0, \boldsymbol{\mu}) = \mathbf{q}_0(\boldsymbol{\mu}), \quad (2.3)$$

where $\mathbf{T} \in \mathbb{R}^{N \times N \times p'}$ is the order-3 tensor satisfying $\mathbf{T}\boldsymbol{\mu}' = \mathbf{A}(\boldsymbol{\mu}) \in \mathbb{R}^{N \times N}$, obtained from the matrix-valued function $\mathbf{A}(\boldsymbol{\mu})$ by tensor-Hom adjunction (i.e., adjointness). In a similar fashion, the ROM (2.2) can be expressed as

$$\dot{\hat{\mathbf{q}}} = \left(\hat{\mathbf{T}}\boldsymbol{\mu}' \right) \hat{\mathbf{q}}, \quad \hat{\mathbf{q}}(0, \boldsymbol{\mu}) = \mathbf{U}^\top \mathbf{M} \mathbf{q}_0(\boldsymbol{\mu}), \quad (2.4a)$$

where $\hat{\mathbf{T}} \in \mathbb{R}^{r \times r \times p'}$ is a reduced order-3 tensor with entries

$$\hat{\mathbf{T}}_{abx} = \sum_{i,j=1}^N U_{ia} \mathbf{T}_{ijx} U_{jb} = \sum_{i,j=1}^N (\mathbf{U}^\top)_{ai} (\mathbf{A}_x)_{ij} (\mathbf{U})_{jb} = (\hat{\mathbf{A}}_x)_{ab}, \quad (2.4b)$$

where $\mathbf{T}_{ijx} = (\mathbf{A}_x)_{ij}$ denotes the (i, j, x) -th entry of \mathbf{T} , U_{ia} denotes the (i, a) -th entry of \mathbf{U} , and $(\hat{\mathbf{A}}_x)_{ab}$ denotes the (a, b) -th entry of $\hat{\mathbf{A}}_x$. Note that $\hat{\mathbf{T}}$ can be viewed as the projection of the full-order tensor \mathbf{T} or, equivalently, as the tensor-Hom adjoint of the projected matrix-valued function $\hat{\mathbf{A}}(\boldsymbol{\mu}) := \sum_{x=1}^{p'} \theta_x(\boldsymbol{\mu}) \hat{\mathbf{A}}_x$. The advantage of the expression (2.4) lies primarily in its compactness: because the explicit tensor contraction $\hat{\mathbf{T}}\boldsymbol{\mu}'$ exposes higher-level structure and removes the need for bookkeeping in terms of the matrices $\hat{\mathbf{A}}_1, \dots, \hat{\mathbf{A}}_{p'}$, additional considerations such as operator symmetries can be more easily included in data-driven ROM construction. Besides leading to a streamlined implementation of the method in [33, 54], this approach also enables simplified proofs of established results (e.g., Corollary 2.1) and facilitates an extension which preserves Hamiltonian structure information (c.f. Section 3).

2.2 Tensor parametric operator inference

The ROM (2.2) is fully and uniquely determined by the entries of the reduced-order matrices $\hat{\mathbf{A}}_1, \dots, \hat{\mathbf{A}}_{p'}$, which in turn depend on the full-order matrices $\mathbf{A}_1, \dots, \mathbf{A}_{p'}$. When these matrices are not available for computation due to, e.g., proprietary or legacy software implementations, an alternative to direct projection is to choose the matrices that minimize the residual of (2.2) with respect to a collection of training states. This is the Operator Inference (OpInf) strategy introduced in [35] and extended to affine-parametric systems in [33, 54]. This section develops a corresponding OpInf procedure for the tensorized ROM (2.4) and presents some analysis of its basic properties.

Suppose access is granted to fixed-time snapshots of the full-order state—solutions to the FOM (2.1)—at N_s training parameter values $\boldsymbol{\mu}_1, \dots, \boldsymbol{\mu}_{N_s} \in \mathbb{R}^p$ and N_t time instances $t_1, \dots, t_{N_t} \in \mathbb{R}$, organized into the state snapshot matrices

$$\mathbf{Q}_s = \begin{bmatrix} \mathbf{q}(t_1, \boldsymbol{\mu}_s) & \cdots & \mathbf{q}(t_{N_t}, \boldsymbol{\mu}_s) \end{bmatrix} \in \mathbb{R}^{N \times N_t}, \quad s = 1, \dots, N_s.$$

Given an \mathbf{M} -orthonormal basis matrix $\mathbf{U} \in \mathbb{R}^{N \times r}$, define the reduced state snapshot matrices $\hat{\mathbf{Q}}_s := \mathbf{U}^\top \mathbf{M} \mathbf{Q}_s \in \mathbb{R}^{r \times N_t}$, $s = 1, \dots, N_s$, as well as corresponding reduced state time derivative matrices $\dot{\hat{\mathbf{Q}}}_s = \mathbf{U}^\top \mathbf{M} D_t(\mathbf{Q}_s) \in \mathbb{R}^{r \times N_t}$, which can be estimated, e.g., via finite difference approximation. Specifically, the α -th column of $\dot{\hat{\mathbf{Q}}}_s$ is an estimate for $\frac{d}{dt} \mathbf{U}^\top \mathbf{M} \mathbf{q}(t, \boldsymbol{\mu}_s)|_{t=t_\alpha}$. A reduced tensor $\bar{\mathbf{T}}$ which approximates the intrusively constructed $\hat{\mathbf{T}}$ in (2.4) can then be inferred by solving the convex minimization problem

$$\arg \min_{\bar{\mathbf{T}}} \frac{1}{2} \sum_{s=1}^{N_s} \left\| \dot{\hat{\mathbf{Q}}}_s - (\bar{\mathbf{T}}\boldsymbol{\mu}'_s) \hat{\mathbf{Q}}_s \right\|^2, \quad (2.5)$$

where $\|\mathbf{F}\|^2 = \sum_{ij} F_{ij} F_{ij}$ denotes the Frobenius matrix norm.

Conveniently, convexity implies that the inference of $\bar{\mathbf{T}}$ in (2.5) is equivalent to a solving a particular linear system. The precise statement of this result is simplified with the following notation: for an order- n tensor $\mathbf{B} \in \mathbb{R}^{N_1 \times N_2 \times \dots \times N_n}$, let $\text{cvec}_{ij} \mathbf{B}, \text{rvec}_{ij} \mathbf{B} \in \mathbb{R}^{N_1 \times \dots \times N_i N_j \times \dots \times N_n}$ denote the partial vectorizations that decrement the tensor degree of \mathbf{B} by unrolling the ordered indices $i < j$ “column-wise” (in the case of cvec_{ij}) or “row-wise” (in the case of rvec_{ij}) into a single index located at the i -th position. More precisely,

indexing the m -th dimension with k_m ,

$$(\text{cvec}_{ij} \mathbf{B})_{k_1, \dots, k_{i-1}, (k_j-1)N_i+k_i, k_{i+1}, \dots, k_{j-1}, k_{j+1}, \dots, k_n} = \mathbf{B}_{k_1, \dots, k_i, \dots, k_j, \dots, k_n}, \quad (2.6a)$$

$$(\text{rvec}_{ij} \mathbf{B})_{k_1, \dots, k_{i-1}, (k_i-1)N_j+k_j, k_{i+1}, \dots, k_{j-1}, k_{j+1}, \dots, k_n} = \mathbf{B}_{k_1, \dots, k_i, \dots, k_j, \dots, k_n}. \quad (2.6b)$$

Additionally, let cmat_{ij} and rmat_{ij} be the natural inverses of cvec_{ij} and rvec_{ij} , i.e.,

$$\text{cmat}_{ij}(\text{cvec}_{ij} \mathbf{B}) = \text{rmat}_{ij}(\text{rvec}_{ij} \mathbf{B}) = \mathbf{B},$$

and let \otimes denote the outer product: for an order- m tensor $\mathbf{A} \in \mathbb{R}^{M_1 \times \dots \times M_m}$ and an order- n tensor $\mathbf{B} \in \mathbb{R}^{N_1 \times \dots \times N_n}$, $\mathbf{A} \otimes \mathbf{B} \in \mathbb{R}^{M_1 \times \dots \times M_m \times N_1 \times \dots \times N_n}$ is a tensor of order $m+n$ with entries

$$(\mathbf{A} \otimes \mathbf{B})_{i_1, \dots, i_m, k_1, \dots, k_n} = A_{i_1, \dots, i_m} B_{k_1, \dots, k_n}.$$

With this notation in place, the following result formulates the inference of $\bar{\mathbf{T}}$ in (2.5) as a system of linear equations.

Theorem 2.1. *Let $\hat{\mathbf{Y}}_s, \hat{\mathbf{Z}}_s \in \mathbb{R}^{r \times N_t}$ and $\boldsymbol{\nu}_s \in \mathbb{R}^{p'}$ for $s = 1, \dots, N_s$. The tensor $\bar{\mathbf{T}} \in \mathbb{R}^{r \times r \times p'}$ minimizes the Lagrangian*

$$L(\bar{\mathbf{T}}) := \frac{1}{2} \sum_{s=1}^{N_s} \left\| \hat{\mathbf{Z}}_s - (\bar{\mathbf{T}} \boldsymbol{\nu}_s) \hat{\mathbf{Y}}_s \right\|^2 \quad (2.7)$$

if and only if $\bar{\mathbf{T}} := \text{cvec}_{23} \bar{\mathbf{T}} \in \mathbb{R}^{r \times r p'}$ satisfies the linear system

$$\hat{\mathbf{B}} \bar{\mathbf{T}}^\top = \hat{\mathbf{C}}^\top, \quad (2.8)$$

where $\hat{\mathbf{B}} \in \mathbb{R}^{r p' \times r p'}$ and $\hat{\mathbf{C}} \in \mathbb{R}^{r \times r p'}$ denote the vectorizations

$$\hat{\mathbf{B}} := \text{rvec}_{12} \text{cvec}_{34} \left(\sum_{s=1}^{N_s} \boldsymbol{\nu}_s \otimes \hat{\mathbf{Y}}_s \hat{\mathbf{Y}}_s^\top \otimes \boldsymbol{\nu}_s \right), \quad \hat{\mathbf{C}} := \text{cvec}_{23} \left(\sum_{s=1}^{N_s} \hat{\mathbf{Z}}_s \hat{\mathbf{Y}}_s^\top \otimes \boldsymbol{\nu}_s \right).$$

Proof. The proof is a direct calculation of the first-order optimality conditions for the Lagrangian (2.7), appealing to a few minor algebraic results detailed in Appendix A. Differentiating L with respect to $\bar{\mathbf{T}}$ and applying the definition of the gradient, it follows that

$$\begin{aligned} dL(\bar{\mathbf{T}}) &= \sum_{s=1}^{N_s} \left\langle (d\bar{\mathbf{T}} \boldsymbol{\nu}_s) \hat{\mathbf{Y}}_s, \hat{\mathbf{Z}}_s - (\bar{\mathbf{T}} \boldsymbol{\nu}_s) \hat{\mathbf{Y}}_s \right\rangle \\ &= \left\langle d\bar{\mathbf{T}}, \sum_{s=1}^{N_s} \left[\hat{\mathbf{Z}}_s - (\bar{\mathbf{T}} \boldsymbol{\nu}_s) \hat{\mathbf{Y}}_s \right] \hat{\mathbf{Y}}_s^\top \otimes \boldsymbol{\nu}_s \right\rangle = \langle d\bar{\mathbf{T}}, \nabla L(\bar{\mathbf{T}}) \rangle, \end{aligned}$$

where $\langle \cdot, \cdot \rangle$ denotes the Frobenius inner product and in which the standard properties listed in Lemma A.1 have been used. Hence, the stationarity condition $\nabla L(\bar{\mathbf{T}}) = \mathbf{0}$ implies the tensorial equation

$$\sum_{s=1}^{N_s} (\bar{\mathbf{T}} \boldsymbol{\nu}_s) \hat{\mathbf{Y}}_s \hat{\mathbf{Y}}_s^\top \otimes \boldsymbol{\nu}_s = \sum_{s=1}^{N_s} \hat{\mathbf{Z}}_s \hat{\mathbf{Y}}_s^\top \otimes \boldsymbol{\nu}_s. \quad (2.9)$$

From Lemma A.2, the left-hand side can be expressed as the tensor contraction

$$\sum_{s=1}^{N_s} (\bar{\mathbf{T}} \boldsymbol{\nu}_s) \hat{\mathbf{Y}}_s \hat{\mathbf{Y}}_s^\top \otimes \boldsymbol{\nu}_s = \bar{\mathbf{T}} : \sum_{s=1}^{N_s} \boldsymbol{\nu}_s \otimes \hat{\mathbf{Y}}_s \hat{\mathbf{Y}}_s^\top \otimes \boldsymbol{\nu}_s,$$

with the convention that $\mathbf{X}_1 : \mathbf{X}_2$ operates over the last two indices of \mathbf{X}_1 and the first two indices of \mathbf{X}_2 in reverse order, i.e., $\mathbf{X}_1 : \mathbf{X}_2 = \sum_{i_{k-1}, i_k} (\mathbf{X}_1)_{\dots i_{k-1} i_k} (\mathbf{X}_2)_{i_k i_{k-1} \dots}$. By Lemma A.3, vectorizing the

Algorithm 2.1 A NumPy/Scipy implementation for inferring a tensor $\bar{\mathbf{T}}$ using the normal equations (2.8) from Theorem 2.1.

```

1 import numpy as np
2 import scipy.linalg as la
3
4 def infer_Tbar_via_normal_eqns(nus, Ys, Zs):
5     p, Ns = nus.shape
6     r, Nt, Ns = Ys.shape # or Zs.shape
7
8     Btsr = np.einsum("xs,ias,jas,ys->xijy", nus, Ys, Ys, nus)
9     Bhat = Btsr.transpose(0, 1, 3, 2).reshape((r*p, r*p), order="C")
10
11     Ctsr = np.einsum("ias,jas,xs->ijx", Zs, Ys, nus)
12     Chat = Ctsr.reshape((r, r*p), order="F")
13
14     Tmat = la.solve(Bhat, Chat.T, assume_a="symmetric").T
15     return Tmat.reshape((r, r, p), order="F")

```

contraction column-wise in $\bar{\mathbf{T}}$ and similarly vectorizing the last two indices of the result transforms the tensorial equation (2.9) into the linear system

$$(\text{cvec}_{23} \bar{\mathbf{T}}) \text{rvec}_{12} \text{cvec}_{34} \left(\sum_{s=1}^{N_s} \boldsymbol{\nu}_s \otimes \hat{\mathbf{Y}}_s \hat{\mathbf{Y}}_s^\top \otimes \boldsymbol{\nu}_s \right) = \text{cvec}_{23} \left(\sum_{s=1}^{N_s} \hat{\mathbf{Z}}_s \hat{\mathbf{Y}}_s^\top \otimes \boldsymbol{\nu}_s \right),$$

which, using the definitions in the statement, is the system $\bar{\mathbf{T}} \hat{\mathbf{B}} = \hat{\mathbf{C}}$. Transposition and the symmetry relationship $\hat{\mathbf{B}}^\top = \hat{\mathbf{B}}$ then yield the linear system (2.8). \square

Theorem 2.1 suggests a straightforward numerical method for solving the tensor parametric OpInf problem (2.5): use the reduced state snapshot matrices to form the linear system (2.8), solve for $\bar{\mathbf{T}}$, then set $\mathbf{T} = \text{cmat}_{23} \bar{\mathbf{T}}$. The resulting non-intrusively obtained OpInf ROM for the approximate state $\hat{\mathbf{q}} = \mathbf{U} \hat{\mathbf{q}}$ is given by

$$\dot{\hat{\mathbf{q}}} = (\bar{\mathbf{T}} \boldsymbol{\mu}') \hat{\mathbf{q}}, \quad \hat{\mathbf{q}}(0, \boldsymbol{\mu}) = \mathbf{U}^\top \mathbf{M} \mathbf{q}_0(\boldsymbol{\mu}). \quad (2.10)$$

This inference procedure can be accomplished with only a few lines of Python code (see Algorithm 2.1) and can be carried out even when data for only $N_s = 1$ parameter sample are available. In such data-scarce settings, however, the uniqueness of the solution is not guaranteed; conditions for uniqueness are established in Corollary 2.1.

The linear system (2.8) can be interpreted as the (vectorized) normal equations for the least-squares problem (2.5), hence Algorithm 2.1 may be disadvantageous if $\hat{\mathbf{B}}$ is poorly conditioned. The following result provides an alternative inference procedure with improved conditioning.

Proposition 2.1. *Let $L : \mathbb{R}^{r \times r \times p'} \rightarrow \mathbb{R}$ be the Lagrangian function (2.7) with argument $\bar{\mathbf{T}} \in \mathbb{R}^{r \times r \times p'}$, defined by the matrices $\hat{\mathbf{Y}}_s, \hat{\mathbf{Z}}_s \in \mathbb{R}^{r \times N_t}$ and vectors $\boldsymbol{\nu}_s \in \mathbb{R}^{p'}$, $s = 1, \dots, N_s$. Consider the tensors $\hat{\mathbf{Y}}, \hat{\mathbf{Z}} \in \mathbb{R}^{r \times N_t \times N_s}$ which result from stacking these matrices along the parameter index, i.e., $\hat{\mathbf{Y}}_{ijk} = (\hat{\mathbf{Y}}_k)_{ij}$ and $\hat{\mathbf{Z}}_{ijk} = (\hat{\mathbf{Z}}_k)_{ij}$. Writing $\bar{\mathbf{O}} = \text{cvec}_{23} \bar{\mathbf{T}} \in \mathbb{R}^{r \times r p'}$, this Lagrangian has the equivalent expression*

$$L(\bar{\mathbf{T}}) = \ell(\bar{\mathbf{O}}) := \|\mathbf{D} \bar{\mathbf{O}}^\top - \mathbf{R}^\top\|^2, \quad (2.11)$$

where $\mathbf{R} = \text{cvec}_{23} \hat{\mathbf{Z}} \in \mathbb{R}^{r \times N_t N_s}$ and $\mathbf{D} = (\text{cvec}_{13} \text{cvec}_{24} \mathbf{K})^\top \in \mathbb{R}^{N_t N_s \times r p'}$ is defined in terms of the order-4 tensor $\mathbf{K} \in \mathbb{R}^{r \times N_t \times p' \times N_s}$ with components $K_{b\alpha x s} = (\hat{\mathbf{Y}}_s)_{b\alpha}(\boldsymbol{\nu}_s)_x$. Moreover, the problem of minimizing the vectorized Lagrangian ℓ decouples over the rows of $\bar{\mathbf{O}}$.

Proof. This can be accomplished by vectorizing the parameter index in L (which was previously summed) and is easiest to express with explicit index manipulations. To that end, define the index ranges

$$\begin{aligned} 1 \leq a, b \leq r, & & 1 \leq \alpha \leq N_t, & & 1 \leq x \leq p', \\ 1 \leq s \leq N_s, & & 1 \leq I \leq N_t N_s, & & 1 \leq Y \leq rp'. \end{aligned}$$

Adopting the Einstein convention where repeated sub- and super-indices imply a summation and letting Σ denote the sum over all remaining free indices, the Lagrangian is expressible as

$$\begin{aligned} L(\bar{\mathbf{T}}) &= \sum \left[(\hat{\mathbf{Z}}_s)_{a\alpha} - \bar{\mathbf{T}}_{abx} (\boldsymbol{\nu}_s)^x (\hat{\mathbf{Y}}_s)^b_{\alpha} \right]^2 = \sum \left[\hat{\mathbf{Z}}_{a\alpha s} - \bar{\mathbf{T}}_{abx} \boldsymbol{\nu}_s^x \hat{\mathbf{Y}}_{\alpha s}^b \right]^2 \\ &= \sum \left[(\text{cvec}_{23} \hat{\mathbf{Z}})_{aI} - (\text{cvec}_{23} \bar{\mathbf{T}})_{aY} (\text{cvec}_{13} \text{cvec}_{24} \mathbf{K})_I^Y \right]^2 = \ell(\bar{\mathbf{O}}), \end{aligned}$$

where the first equality is the definition of the Lagrangian, the second uses the definition of the tensors $\hat{\mathbf{Y}}, \hat{\mathbf{Z}}$, the third vectorizes the double contraction and its result while applying the definition of \mathbf{K} , and the fourth transposes the expression under the norm. Applying the definitions of $\mathbf{D}, \bar{\mathbf{O}}$, and \mathbf{R} , it follows that

$$\ell(\bar{\mathbf{O}}) = \|\mathbf{R} - \bar{\mathbf{O}}\mathbf{D}^\top\|^2 = \|\mathbf{D}\bar{\mathbf{O}}^\top - \mathbf{R}^\top\|^2,$$

as desired. Moreover, the minimization problem decouples over the rows $\bar{\mathbf{o}}^a \in \mathbb{R}^{rp'}$ of $\bar{\mathbf{O}}$ and $\mathbf{r}^a \in \mathbb{R}^{N_t N_s}$ of \mathbf{R} , $a = 1, \dots, r$, into r independent least-squares problems, i.e.,

$$\arg \min_{\bar{\mathbf{O}}} \ell(\bar{\mathbf{O}}) = \left\{ \arg \min_{\bar{\mathbf{o}}^a} \|\mathbf{D}\bar{\mathbf{o}}^a - \mathbf{r}^a\|^2 \right\}_{a=1}^r. \quad (2.12)$$

where each sub-problem has $N_t N_s$ data points and rp' unknowns. \square

Proposition 2.1 shows that the least-squares problem (2.11) is equivalent to the system of normal equations (2.8). Indeed, $\mathbf{D}^\top \mathbf{D} = \hat{\mathbf{B}}$, which can be seen by considering the tensor $\mathbf{X} \in \mathbb{R}^{r \times p \times r \times p}$ with components

$$X_{axyb} = \sum_{\alpha, s} K_{a\alpha x s} K_{b\alpha y s} = \sum_{\alpha, s} (\hat{\mathbf{Y}}_s)_{a\alpha} (\boldsymbol{\nu}_s)_x (\hat{\mathbf{Y}}_s)_{b\alpha} (\boldsymbol{\nu}_s)_y = \sum_s (\boldsymbol{\nu}_s)_x (\hat{\mathbf{Y}}_s \hat{\mathbf{Y}}_s^\top)_{ab} (\boldsymbol{\nu}_s)_y.$$

The matrix $\hat{\mathbf{B}}$ is a partial vectorization of this quantity; specifically,

$$\hat{\mathbf{B}} = \text{rvec}_{12} \text{cvec}_{34} (\text{perm}_{12} \mathbf{X}) = \text{cvec}_{12} \text{cvec}_{34} \mathbf{X} = \mathbf{D}^\top \mathbf{D},$$

since $\text{rvec}_{ij} \text{perm}_{ij} = \text{cvec}_{ij}$, where perm_{ij} denotes a permutation of indices i and j . This implies that the condition number of \mathbf{D} is the square root of the condition number of $\hat{\mathbf{B}}$, hence the direct minimization of (2.11) via, e.g., QR factorization of \mathbf{D} , is more numerically viable than solving (2.8). Additionally, iterative approaches based on low-rank factorizations of \mathbf{D} can be used to implicitly regularize and efficiently solve the inference problem. A naïve implementation of this procedure using direct minimization is presented in Algorithm 2.2.

The expressions in Proposition 2.1 involving $\mathbf{D}, \bar{\mathbf{O}}$, and \mathbf{R} exactly correspond to the state-linear parts of the inference problem (2.13) in previous work [33]. The advantage of Algorithm 2.2, in addition to the brevity of the implementation, is that the expression for \mathbf{D} in Proposition 2.1 provides insight into when the inference of $\bar{\mathbf{T}}$ in (2.5) has a unique solution. This is evidenced by the following concise result, analogous to [33, Theorem 2.3].

Corollary 2.1. *Let \mathbf{D}, \mathbf{R} , and $\ell(\bar{\mathbf{O}})$ be as in Proposition 2.1. Let $\boldsymbol{\Theta} \in \mathbb{R}^{N_s \times p'}$ be the matrix with entries $\Theta_{sx} = (\boldsymbol{\nu}_s)_x$. The inference problem $\arg \min \ell(\bar{\mathbf{O}})$ in (2.12) has a unique solution $\bar{\mathbf{O}} = \text{cvec}_{23} \bar{\mathbf{T}}$ if and only if both $\boldsymbol{\Theta}$ and $(\text{cvec}_{23} \hat{\mathbf{Y}})^\top \in \mathbb{R}^{N_t N_s \times r}$ have full column rank.*

Proof. Similar to Proposition 2.1, write $\mathbf{D} = (\text{cvec}_{13} \text{cvec}_{24} \mathbf{K})^\top \in \mathbb{R}^{N_t N_s \times rp'}$, where the tensor $\mathbf{K} \in \mathbb{R}^{r \times N_t \times p' \times N_s}$ has components $K_{b\alpha x s} = (\hat{\mathbf{Y}}_s)_{b\alpha} \Theta_{sx}$. Note that \mathbf{K} ‘‘factors’’ as the combination tensor-Hadamard product of $\hat{\mathbf{Y}}$ and $\mathbf{1} \otimes \boldsymbol{\Theta}^\top$: it is an outer product in the indices b, x and a Hadamard product in

Algorithm 2.2 A NumPy implementation for inferring a tensor $\bar{\mathbf{T}}$ using the least-squares problem (2.11) from Proposition 2.1.

```

1 import numpy as np
2
3 def infer_Tbar_with_lstsq(nus, Ys, Zs):
4     p, Ns = nus.shape
5     r, Nt, Ns = Bs.shape # or Zs.shape
6
7     K = np.einsum("ias,xs->iaxs", Ys, nus)
8     Dt = K.transpose((0, 2, 1, 3)).reshape((r*p, Nt*Ns), order="F")
9     R = Zs.reshape((r, Nt*Ns), order="F")
10
11     Obar = np.linalg.lstsq(Dt.T, R.T)[0].T
12     return Obar.reshape((r, r, p), order="F")

```

the indices α, s . This implies that, for any $\mathbf{v} \in \mathbb{R}^{rp'}$ in the kernel of \mathbf{D} , (Einstein summation assumed)

$$\begin{aligned}
(\text{cmat}_{12} \mathbf{D}\mathbf{v})_{\alpha s} &= (\text{cmat}_{12} [\text{cmat}_{34} \mathbf{D} : \text{cmat}_{12} \mathbf{v}^T])_{\alpha s} = \hat{Y}_{b\alpha s} \Theta_{sx} (\text{cmat}_{12} \mathbf{v})^{bx} \\
&= \hat{Y}_{b\alpha s} \Theta_{sx} (v^{ay} \mathbf{e}_a \mathbf{e}_y^T)^{bx} = v^{ay} \hat{Y}_{b\alpha s} \Theta_{sx} \delta_a^b \delta_y^x \\
&= (\hat{Y}_{a\alpha s} v^{ay}) \Theta_{sy} = \hat{Y}_{a\alpha s} (v^{ay} \Theta_{sy}) = 0.
\end{aligned}$$

If Θ has full column rank, the first equality on the last line shows that $(\text{cvec}_{23} \hat{\mathbf{Y}})^T$ is rank-deficient. Similarly, if $(\text{cvec}_{23} \hat{\mathbf{Y}})^T$ has full column rank, the second equality on the last line shows that Θ is rank-deficient. Therefore, \mathbf{D} has full column rank whenever these matrices do, while if either is rank deficient, then so is \mathbf{D} . \square

Remark 2.2 (Nonlinear terms). Tensor parametric OpInf can be extended in a straightforward manner to account for quadratic (or higher-order) polynomial terms $\mathbf{H}(\boldsymbol{\mu}) : (\mathbf{q} \otimes \mathbf{q})$ with affine parameter dependence appearing in (2.1), such as those seen in [33]. In this case, a tensor \mathbf{T} satisfying $\mathbf{H}(\boldsymbol{\mu}) = \mathbf{T}\boldsymbol{\mu}'$ must have order 4, as \mathbf{H} (if not matricized) is of order 3. Since higher-order terms are not necessary for the numerical examples presented later, such extensions are left for future work.

The results of this section demonstrate how solutions to the tensor parametric OpInf problem are global minima and how the tensor reformulation clearly and concisely recovers previous parametric OpInf formulations. Before discussing how this approach also enables a novel extension to systems with Hamiltonian structure, an example is presented to illustrate its practical utility.

2.3 Example: Heat equation

Let $\Omega \subset \mathbb{R}^d$ where $d \in \{1, 2, 3\}$ and consider the following initial value problem with homogeneous Dirichlet boundary conditions,

$$\begin{cases} \dot{q}(\mathbf{x}, t) = \nabla \cdot (c(\mathbf{x}, \boldsymbol{\mu}) \nabla q(\mathbf{x}, t)), & \mathbf{x} \in \Omega \times (0, t_f], \\ q(\mathbf{x}, 0) = q_0(\mathbf{x}), & \mathbf{x} \in \Omega, \\ q(\mathbf{x}, t) = 0, & \mathbf{x} \in \partial\Omega \times (0, t_f], \end{cases} \quad (2.13)$$

where $q : \Omega \times (0, t_f) \rightarrow \mathbb{R}$ is the continuous system state, $c : \Omega \times \mathbb{R}^p \rightarrow \mathbb{R}$ is the parameterized thermal conductivity coefficient, and $q_0 : \Omega \rightarrow \mathbb{R}$ is a given initial condition. Note that q depends implicitly on the conductivity parameters $\boldsymbol{\mu}$. Let $\Omega = \bigcup_{i=1}^p \Omega_i$ be a non-overlapping decomposition of the spatial domain and consider the piecewise-continuous $c(\mathbf{x}, \boldsymbol{\mu})$ given by

$$c(\mathbf{x}, \boldsymbol{\mu}) = [\mathbf{x} \in \Omega_1] \mu_1 + [\mathbf{x} \in \Omega_2] \mu_2 + \dots + [\mathbf{x} \in \Omega_p] \mu_p, \quad \boldsymbol{\mu} = [\mu_1 \ \mu_2 \ \dots \ \mu_p]^T,$$

where $[S]$ is the Iverson bracket [29], i.e., the indicator function of the statement S .

A finite-element-based FOM for (2.13) can be readily constructed using a continuous Galerkin discretization in space. Let $\Omega_h := \{K_i\}_{i=1}^{N_E}$ be a conforming triangulation of the domain Ω containing N_E elements. The Galerkin weak formulation of (2.13) with this spatial discretization is the following: find $\dot{q}_h \in V_h$ such that for all $v_h \in V_h$,

$$(\dot{q}_h, v_h)_{\Omega_h} = -(c(\cdot, \boldsymbol{\mu}) \nabla q_h, \nabla v_h)_{\Omega_h}, \quad (2.14)$$

where $(\cdot, \cdot)_{\Omega_h}$ denotes the L^2 inner product on Ω_h and V_h is the $H^1(\Omega)$ -conforming finite element space

$$V_h := \{v_h \in H^1(\Omega) : v_h|_K \in P_1(K), \forall K \in \Omega_h; v_h|_{\partial\Omega} = 0\},$$

with $P_1(K)$ representing the space of linear polynomials on element K . Given a basis $\{\phi_i\}_{i=1}^N$ for V_h , inserting the approximation $q(\mathbf{x}, t) \approx q_h(\mathbf{x}, t) := \sum_{i=1}^N q_i(t) \phi_i(\mathbf{x})$ into (2.14) leads to the system of N ODEs $\mathbf{M} \dot{\mathbf{q}} = \mathbf{A}(\boldsymbol{\mu}) \mathbf{q}$ with matrix entries

$$\begin{aligned} (\mathbf{M})_{ij} &= (\phi_i, \phi_j)_{\Omega_h}, \\ (\mathbf{A}(\boldsymbol{\mu}))_{ij} &= -(c(\cdot, \boldsymbol{\mu}) \nabla \phi_i, \nabla \phi_j)_{\Omega_h} = - \sum_{x=1}^p \mu_x (\nabla \phi_i, \nabla \phi_j)_{\Omega_x}. \end{aligned} \quad (2.15a)$$

The corresponding tensorized FOM $\mathbf{M} \dot{\mathbf{q}} = (\mathbf{T} \boldsymbol{\mu}') \mathbf{q}$ has tensor entries

$$\mathbb{T}_{ijk} = ([\mathbf{x} \in \Omega_k] \nabla \phi_i, \nabla \phi_j)_{\Omega_h} = (\nabla \phi_i, \nabla \phi_j)_{\Omega_k}. \quad (2.15b)$$

Given snapshot matrices $\mathbf{Q}_1, \dots, \mathbf{Q}_{N_s}$, Algorithm 2.1 or Algorithm 2.2 can now be used with data $\mathbf{Y}_s = \mathbf{U}^\top \mathbf{M} \mathbf{Q}_s$ and $\mathbf{Z}_s = \mathbf{U}^\top \mathbf{M} D_t(\mathbf{Q}_s)$ to infer a reduced tensor $\bar{\mathbf{T}} \approx \hat{\mathbf{T}}$, producing a parametric OpInf ROM $\dot{\hat{\mathbf{q}}} = (\bar{\mathbf{T}} \boldsymbol{\mu}') \hat{\mathbf{q}}$.

Remark 2.3 (Tensor symmetry). The full-order tensor \mathbf{T} in (2.15b) is symmetric in its first two indices, reflecting the fact that the heat equation (2.13) is an L^2 -gradient flow. However, Algorithm 2.1 and Algorithm 2.2 do not enforce this symmetry as a constraint, i.e., the learned tensor $\bar{\mathbf{T}}$ is not necessarily symmetric in its first two indices. The next section develops a tensor parametric OpInf algorithm with additional constraints that preserve symmetric (or anti-symmetric) tensor structure.

3 Tensor parametric operator inference for Hamiltonian systems

The concise tensor formulation developed in Section 2 enables a principled extension to parametric Hamiltonian systems, where preservation of additional algebraic structure in the learned tensor $\bar{\mathbf{T}} \approx \hat{\mathbf{T}}$ is necessary in order to enable the energy-conservative and symplectic characteristics of Hamiltonian dynamics. Section 3.1 summarizes the key aspects of Hamiltonian model reduction, and Section 3.2 develops an analog to Algorithm 2.1 that accounts for the additional desired structure. An application to wave phenomena is outlined in Section 3.3.

3.1 Hamiltonian model reduction

Canonical Hamiltonian systems are defined by the joint state variable $\mathbf{y} = [\mathbf{q}^\top \ \mathbf{p}^\top]^\top \in \mathbb{R}^{2N}$, a Hamiltonian functional $H : \mathbb{R}^{2N} \rightarrow \mathbb{R}$ representing a notion of energy, and a skew-adjoint block matrix $\mathbf{J} = -\mathbf{J}^\top \in \mathbb{R}^{2N \times 2N}$ encoding the symplectic structure:

$$\dot{\mathbf{y}} = \{\mathbf{y}, H(\mathbf{y})\} = \mathbf{J} \nabla H(\mathbf{y}), \quad \mathbf{J} = \begin{bmatrix} \mathbf{0} & \mathbf{I} \\ -\mathbf{I} & \mathbf{0} \end{bmatrix}. \quad (3.1)$$

Here, $\{F, G\} = \nabla F \cdot \mathbf{J} \nabla G$ is a particular Lie algebra realization on functions known as the (canonical) Poisson bracket, and notation has been slightly abused by vectorizing this bracket over the components of

the state \mathbf{y} . A core feature of Hamiltonian systems is that their solutions conserve energy for all time, which can be seen by computing the rate of change in H ,

$$\begin{aligned}\dot{H}(\mathbf{y}) &= \dot{\mathbf{y}}^\top \nabla H(\mathbf{y}) = \nabla H(\mathbf{y})^\top \mathbf{J}^\top \nabla H(\mathbf{y}) = -\nabla H(\mathbf{y})^\top \mathbf{J} \nabla H(\mathbf{y}) \\ &= (\nabla H(\mathbf{y})^\top \mathbf{J}^\top \nabla H(\mathbf{y}))^\top = \nabla H(\mathbf{y})^\top \mathbf{J} \nabla H(\mathbf{y}),\end{aligned}$$

which shows that $\dot{H}(\mathbf{y}) = 0$ for all \mathbf{y} . This reflects the fact that Hamiltonian systems yield symplectic gradient flows whose solutions are confined to individual level sets of H [31].

When Hamiltonian systems are discretized with the finite element method, it is typical to incorporate a symmetric positive definite mass matrix $\mathbf{M} \in \mathbb{R}^{2N \times 2N}$, leading to models of the form

$$\mathbf{M}\dot{\mathbf{y}} = \mathbf{L}\mathbf{M}^{-1}\nabla H(\mathbf{y}), \quad \mathbf{L}^\top = -\mathbf{L}. \quad (3.2)$$

To expose the Hamiltonian structure of this system, define $\bar{\mathbf{J}} = \mathbf{M}^{-1}\mathbf{L}$ and write

$$\dot{\mathbf{y}} = \mathbf{M}^{-1}\mathbf{L}\mathbf{M}^{-1}\nabla H(\mathbf{y}) = \bar{\mathbf{J}}\nabla^M H(\mathbf{y}), \quad (3.3)$$

where $\nabla^M H = \mathbf{M}^{-1}\nabla H$ is the gradient of H with respect to the weighted inner product $\mathbf{a}^* \mathbf{b} = \mathbf{a}^\top \mathbf{M} \mathbf{b}$ induced by \mathbf{M} (see Appendix B). The adjoint of $\bar{\mathbf{J}}$ in this inner product is given by

$$\bar{\mathbf{J}}^* = (\mathbf{M}^{-1}\mathbf{L})^* = \mathbf{M}^{-1}(\mathbf{M}^{-1}\mathbf{L})^\top \mathbf{M} = \mathbf{M}^{-1}\mathbf{L}^\top \mathbf{M}^{-\top} \mathbf{M} = -\mathbf{M}^{-1}\mathbf{L} = -\bar{\mathbf{J}}.$$

Therefore, $\bar{\mathbf{J}}$ is skew-adjoint with respect to \mathbf{M} , hence (3.3) is a Hamiltonian system in the \mathbf{M} -weighted inner product. Additionally, H is conserved along solutions:

$$\dot{H}(\mathbf{y}) = \dot{\mathbf{y}}^* \nabla^M H(\mathbf{y}) = (\bar{\mathbf{J}} \nabla^M H(\mathbf{y}))^* \nabla^M H(\mathbf{y}) = -\nabla^M H(\mathbf{y})^* (\bar{\mathbf{J}} \nabla^M H(\mathbf{y})) = 0.$$

Remark 3.1 (Block diagonal mass). It is often the case that $\mathbf{L} = \mathbf{J}\mathbf{M}$ and that the mass matrix \mathbf{M} can be written as $\mathbf{M} = \text{blockdiag}(\mathbf{M}_q, \mathbf{M}_p)$, where $\mathbf{M}_q \in \mathbb{R}^{N \times N}$ is a symmetric positive definite mass matrix corresponding to \mathbf{q} and \mathbf{p} . In this case, $\mathbf{J}\mathbf{M} = \mathbf{M}\mathbf{J}$ and, hence, $\bar{\mathbf{J}} = \mathbf{M}^{-1}\mathbf{L} = \mathbf{M}^{-1}\mathbf{J}\mathbf{M} = \mathbf{J}$. For the remainder of this section, \mathbf{J} is written instead of $\bar{\mathbf{J}}$ and it is assumed that $\mathbf{J}^* = -\mathbf{J}$.

The effectiveness of Hamiltonian systems in modeling non-dissipative phenomena has motivated a significant amount of work into their model reduction [1, 8, 21, 22, 25, 36, 45, 47]. The key observation is that Hamiltonian systems are governed by a variational principle, and violation of this principle at the reduced-order level leads quickly to unphysical results, especially in the predictive regime where ROMs are intended to provide computational savings (see, e.g., [21, Figure 10]). Effective ROMs for Hamiltonian systems—whether intrusive or non-intrusive—must therefore preserve the Hamiltonian structure, meaning that the reduced dynamics should be governed by an appropriate reduced Hamiltonian function $\hat{H} : \mathbb{R}^{2r} \rightarrow \mathbb{R}$ and reduced skew-adjoint matrix $\hat{\mathbf{J}} : \mathbb{R}^{2r \times 2r}$.¹

Structure preservation is equally critical in ROMs for *parametric* Hamiltonian systems, i.e., those governed by a parameterized Hamiltonian $H = H(\mathbf{y}, \boldsymbol{\mu})$. In this case, the ROM must be defined in terms of the gradient of an appropriate reduced parameterized Hamiltonian. To this end, consider the Hamiltonian

$$H(\mathbf{y}, \boldsymbol{\mu}) = \frac{1}{2} \mathbf{y}^* \mathbf{A}(\boldsymbol{\mu}) \mathbf{y} + f(\mathbf{y}, \boldsymbol{\mu}), \quad (3.4)$$

defined in terms of a nonlinear function $f : \mathbb{R}^{2N} \times \mathbb{R}^p \rightarrow \mathbb{R}$ and a matrix field $\mathbf{A} : \mathbb{R}^p \rightarrow \mathbb{R}^{2N \times 2N}$ with affine parametric dependence. The (canonical) Hamiltonian system generated by H takes the form

$$\dot{\mathbf{y}} = \mathbf{J} \nabla^M H(\mathbf{y}, \boldsymbol{\mu}) = \mathbf{J}(\mathbf{A}(\boldsymbol{\mu}) \mathbf{y} + \nabla^M f(\mathbf{y}, \boldsymbol{\mu})). \quad (3.5)$$

It may be assumed that $\mathbf{A}(\boldsymbol{\mu})$ is self-adjoint, that is, $\mathbf{A}(\boldsymbol{\mu}) = \mathbf{A}(\boldsymbol{\mu})^* = \mathbf{M}^{-1} \mathbf{A}^\top(\boldsymbol{\mu}) \mathbf{M}$, since only the self-adjoint part of $\mathbf{A}(\boldsymbol{\mu})$ contributes to the value of H (see Lemmata B.1 and B.4). Since \mathbf{A} depends affinely on $\boldsymbol{\mu}$, it follows as before that $\mathbf{A}(\boldsymbol{\mu}) = \mathbf{T} \boldsymbol{\mu}'$ for some constant tensor $\mathbf{T} \in \mathbb{R}^{2N \times 2N \times p'}$ and a vector

¹In fact, $\hat{\mathbf{J}} = \hat{\mathbf{J}}(\mathbf{y})$ can generally be a matrix field, and not all skew-adjoint $\hat{\mathbf{J}}$ define valid Hamiltonian systems. More details can be found in, e.g., [21, 22].

$\boldsymbol{\mu}' = \boldsymbol{\theta}(\boldsymbol{\mu}) \in \mathbb{R}^{p'}$. Additionally, because $\mathbf{A}(\boldsymbol{\mu})$ is self-adjoint, it follows that \mathbf{T} is self-adjoint in its first two indices, denoted $\mathbf{T}^* = \mathbf{T}$. The key to the tensor parametric Hamiltonian OpInf developed here will be an inference procedure analogous to Algorithm 2.1 which explicitly takes this symmetry into account.

To see the constraints that Hamiltonian structure places at the reduced-order level, consider (3.5) with $f \equiv 0$ and a known initial condition:

$$\dot{\mathbf{y}} = \mathbf{J}\mathbf{A}(\boldsymbol{\mu})\mathbf{y} = \mathbf{J}(\mathbf{T}\boldsymbol{\mu}')\mathbf{y}, \quad \mathbf{y}(0, \boldsymbol{\mu}) = \mathbf{y}_0(\boldsymbol{\mu}). \quad (3.6)$$

Given a trial space basis $\mathbf{U} \in \mathbb{R}^{2N \times 2r}$ which is metric-compatible in the sense that $\mathbf{U}^*\mathbf{U} = \hat{\mathbf{M}}\mathbf{U}^\top\mathbf{M}\mathbf{U} = \mathbf{I}$ for some $\hat{\mathbf{M}} \in \mathbb{R}^{2r \times 2r}$ defining an inner product on the reduced coordinates (typically $\hat{\mathbf{M}} = \mathbf{I}$), making the approximation $\tilde{\mathbf{y}} := \mathbf{U}\hat{\mathbf{y}} \approx \mathbf{y}$ with $\hat{\mathbf{y}} = \hat{\mathbf{y}}(t, \boldsymbol{\mu}) \in \mathbb{R}^{2r}$ and performing \mathbf{M} -orthogonal projection in (3.6) results in the following (intrusive) ROM:

$$\dot{\hat{\mathbf{y}}} = \mathbf{U}^*\mathbf{J}(\mathbf{T}\boldsymbol{\mu}')\mathbf{U}\hat{\mathbf{y}}, \quad \hat{\mathbf{y}}(0, \boldsymbol{\mu}) = \mathbf{U}^*\mathbf{y}_0(\boldsymbol{\mu}). \quad (3.7)$$

Unfortunately, the ROM (3.7) is not Hamiltonian with respect to the reduced inner product $\hat{\mathbf{a}}^*\hat{\mathbf{b}} = \hat{\mathbf{a}}^\top\hat{\mathbf{M}}\hat{\mathbf{b}}$ since $(\mathbf{U}^*\mathbf{J})^* = \mathbf{J}^*\mathbf{U} = -\mathbf{J}\mathbf{U} \neq -\mathbf{U}^*\mathbf{J}$, which implies that the symplectic structure of the original system is lost. Moreover, the natural reduced Hamiltonian functional $\hat{H}(\hat{\mathbf{y}}, \boldsymbol{\mu}') := H(\mathbf{U}\hat{\mathbf{y}}, \boldsymbol{\mu})$ is not conserved: for any $\boldsymbol{\mu}' \in \mathbb{R}^{p'}$,

$$\begin{aligned} \dot{\hat{H}}(\hat{\mathbf{y}}, \boldsymbol{\mu}') &= \dot{\hat{\mathbf{y}}}^*\nabla^{\hat{\mathbf{M}}}\hat{H}(\hat{\mathbf{y}}) = (\mathbf{U}^*\mathbf{J}(\mathbf{T}\boldsymbol{\mu}')\mathbf{U}\hat{\mathbf{y}})^*\mathbf{U}^*(\mathbf{T}\boldsymbol{\mu}')\mathbf{U}\hat{\mathbf{y}} \\ &= -((\mathbf{T}\boldsymbol{\mu}')\mathbf{U}\hat{\mathbf{y}})^*\mathbf{J}\mathbf{U}\mathbf{U}^*(\mathbf{T}\boldsymbol{\mu}')\mathbf{U}\hat{\mathbf{y}} \neq 0. \end{aligned}$$

In other words, the structural and conservative properties of the FOM (3.6) are not automatically inherited by the projection-based ROM (3.7), and solutions of (3.7) are liable to exhibit artificial energetic profiles and stability issues.

There are two primary approaches to circumventing this defect: modifying the reduced basis \mathbf{U} , or modifying the equation form (3.7). The first approach was initiated by the work [36], which introduced the Proper Symplectic Decomposition (PSD) for building Hamiltonian ROMs. This involves constructing a basis $\mathbf{U} \in \mathbb{R}^{2N \times 2r}$ with the desirable \mathbf{J} -equivariance property $\mathbf{U}^*\mathbf{J} = \hat{\mathbf{J}}\mathbf{U}^*$, where $\hat{\mathbf{J}} = -\hat{\mathbf{J}}^* \in \mathbb{R}^{2r \times 2r}$. The advantage of this property is that a variationally consistent and canonical Hamiltonian ROM follows directly from Galerkin projection onto the span of \mathbf{U} ,

$$\dot{\hat{\mathbf{y}}} = \mathbf{U}^*\mathbf{J}(\mathbf{T}\boldsymbol{\mu}')\mathbf{U}\hat{\mathbf{y}} = \hat{\mathbf{J}}\mathbf{U}^*(\mathbf{T}\boldsymbol{\mu}')\mathbf{U}\hat{\mathbf{y}} = \hat{\mathbf{J}}(\hat{\mathbf{T}}\boldsymbol{\mu}')\hat{\mathbf{y}}, \quad (3.8)$$

where the reduced tensor $\hat{\mathbf{T}} \in \mathbb{R}^{2r \times 2r \times p'}$ is (assuming $\hat{\mathbf{M}} = \mathbf{I}$) symmetric in its first two indices, written $\hat{\mathbf{T}} = \hat{\mathbf{T}}^\top$, and $(\hat{\mathbf{T}}\boldsymbol{\mu}')\hat{\mathbf{y}} = \nabla\hat{H}(\hat{\mathbf{y}}, \boldsymbol{\mu})$ is the (Euclidean) gradient of the reduced Hamiltonian $\hat{H}(\hat{\mathbf{y}}, \boldsymbol{\mu}') = (1/2)\hat{\mathbf{y}}^\top(\hat{\mathbf{T}}\boldsymbol{\mu}')\hat{\mathbf{y}}$. This intrusively constructed ROM exactly preserves the reduced Hamiltonian \hat{H} , since

$$\dot{\hat{H}}(\hat{\mathbf{y}}, \boldsymbol{\mu}') = \hat{\mathbf{y}}^\top\nabla\hat{H}(\hat{\mathbf{y}}, \boldsymbol{\mu}') = \hat{\mathbf{y}}^\top(\hat{\mathbf{T}}\boldsymbol{\mu}')^\top\hat{\mathbf{J}}^\top(\hat{\mathbf{T}}\boldsymbol{\mu}')\hat{\mathbf{y}} = -\hat{\mathbf{y}}^\top(\hat{\mathbf{T}}\boldsymbol{\mu}')^\top\hat{\mathbf{J}}(\hat{\mathbf{T}}\boldsymbol{\mu}')\hat{\mathbf{y}} = 0.$$

Mirroring this structure, an appropriate OpInf ROM for (3.6) that incorporates the dynamics induced by the Hamiltonian used above is

$$\dot{\hat{\mathbf{y}}} = \hat{\mathbf{J}}(\bar{\mathbf{T}}\boldsymbol{\mu}')\hat{\mathbf{y}}, \quad \hat{\mathbf{y}}(0, \boldsymbol{\mu}) = \mathbf{U}^*\mathbf{y}_0(\boldsymbol{\mu}), \quad (3.9)$$

as long as the inferred tensor $\bar{\mathbf{T}}$ is constrained to satisfy the symmetry property $\bar{\mathbf{T}}^\top = \bar{\mathbf{T}}$. Similar to the previous computation, it is straightforward to verify that the ROM (3.9) exactly preserves the reduced Hamiltonian $\bar{H}(\hat{\mathbf{y}}, \boldsymbol{\mu}') = (1/2)\hat{\mathbf{y}}^\top(\bar{\mathbf{T}}\boldsymbol{\mu}')\hat{\mathbf{y}}$, which approximates $\hat{H}(\hat{\mathbf{y}}, \boldsymbol{\mu})$. The next section extends the work of Section 2 to infer Hamiltonian ROMs of the form (3.9) in a non-intrusive fashion.

The alternative to designing the basis matrix \mathbf{U} to satisfy the potentially restrictive \mathbf{J} -equivariance property is to modify the model form (3.7). An effective way of accomplishing this while retaining variational consistency was presented in [22], which applies Petrov–Galerkin projection onto the test space $\mathbf{J}\mathbf{U}$. Applying $(\mathbf{J}\mathbf{U})^*$ to both sides of (3.6) yields

$$\dot{\hat{\mathbf{y}}} = \hat{\mathbf{J}}^{-\top}\nabla\hat{H}(\hat{\mathbf{y}}, \boldsymbol{\mu}') = \hat{\mathbf{J}}^{-\top}(\hat{\mathbf{T}}\boldsymbol{\mu}')\hat{\mathbf{y}}, \quad (3.10)$$

which satisfies $\hat{\mathbf{T}}^\top = \hat{\mathbf{T}}$ and is symplectic since $\hat{\mathbf{J}}^{-\top} = (\mathbf{U}^*\mathbf{J}\mathbf{U})^{-\top} = -\hat{\mathbf{J}}^{-1}$ is constant in the state.²

²The fact that $\hat{\mathbf{J}}^{-\top}$ is constant implies that the Jacobi identity reduces to the symmetry condition $\hat{\mathbf{J}}^{-\top} = -\hat{\mathbf{J}}^{-1}$.

Like (3.8), this ROM conserves the reduced Hamiltonian $\hat{H}(\hat{\mathbf{y}}, \boldsymbol{\mu})$.

3.2 Enforcing symmetries in tensor parametric operator inference

A key feature of the canonical Hamiltonian ROMs (3.8)–(3.10) is the preservation of the symmetry condition $\hat{\mathbf{A}}(\boldsymbol{\mu})^\top = \hat{\mathbf{A}}(\boldsymbol{\mu})$ governing the reduced Hamiltonian \hat{H} . In the case of affine parameter dependence, this reduces to the symmetry constraint $\hat{\mathbf{T}}^\top = \hat{\mathbf{T}}$ on the first two indices of the tensor representation $\hat{\mathbf{T}}\boldsymbol{\mu}' = \hat{\mathbf{A}}(\boldsymbol{\mu})$. The natural extension of the tensor OpInf problem (2.10) to this setting is the following constrained regression problem:

$$\arg \min_{\bar{\mathbf{T}}} \frac{1}{2} \sum_{s=1}^{N_s} \left\| \dot{\hat{\mathbf{Q}}}_s - \hat{\mathbf{J}}(\bar{\mathbf{T}}\boldsymbol{\mu}'_s) \hat{\mathbf{Q}}_s \right\|^2 \quad \text{s.t.} \quad \bar{\mathbf{T}}^\top = \bar{\mathbf{T}}, \quad (3.11)$$

where, as in the setting of Section 2, $\hat{\mathbf{Q}}_s, \dot{\hat{\mathbf{Q}}}_s \in \mathbb{R}^{2r \times N_t}$ are reduced state snapshot matrices and (approximate) reduced state time derivative matrices corresponding to parameter samples $\boldsymbol{\mu}_s \in \mathbb{R}^{p'}$, $s = 1, \dots, N_s$. The following theorem provides a compact strategy for solving this problem.

Theorem 3.1. *Let $\hat{\mathbf{X}}_s \in \mathbb{R}^{r \times r}$, $\hat{\mathbf{Y}}_s \in \mathbb{R}^{r \times N_t}$, $\hat{\mathbf{Z}}_s \in \mathbb{R}^{r \times N_t}$, and $\boldsymbol{\nu}_s \in \mathbb{R}^{p'}$ for $s = 1, \dots, N_s$. Then solutions to the convex minimization problem*

$$\arg \min_{\bar{\mathbf{T}}} \frac{1}{2} \sum_{s=1}^{N_s} \left\| \hat{\mathbf{Z}}_s - \hat{\mathbf{X}}_s(\bar{\mathbf{T}}\boldsymbol{\nu}_s) \hat{\mathbf{Y}}_s \right\|^2 \quad \text{s.t.} \quad \bar{\mathbf{T}}\boldsymbol{\eta} = \pm(\bar{\mathbf{T}}\boldsymbol{\eta})^\top \quad \forall \boldsymbol{\eta} \in \mathbb{R}^{p'},$$

can be computed by solving the linear system

$$\begin{aligned} \sum_{s=1}^{N_s} \left[\boldsymbol{\nu}_s \boldsymbol{\nu}_s^\top \otimes_K \left(\hat{\mathbf{X}}_s^\top \hat{\mathbf{X}}_s \oplus_K \hat{\mathbf{Y}}_s \hat{\mathbf{Y}}_s^\top \right) \right] \text{vec } \bar{\mathbf{T}} \\ = \sum_{s=1}^{N_s} \boldsymbol{\nu}_s \otimes_K \text{cvec}_{12} \left(\hat{\mathbf{X}}_s^\top \hat{\mathbf{Z}}_s \hat{\mathbf{Y}}_s^\top \pm \hat{\mathbf{Y}}_s \hat{\mathbf{Z}}_s^\top \hat{\mathbf{X}}_s \right), \end{aligned} \quad (3.12)$$

where $\text{vec } \bar{\mathbf{T}} = \text{cvec}_{12}(\text{cvec}_{12} \bar{\mathbf{T}})$ is a total column-wise flattening of the tensor $\bar{\mathbf{T}} \in \mathbb{R}^{r \times r \times p'}$, $\mathbf{X} \otimes_K \mathbf{Y} = \text{rvec}_{13} \text{rvec}_{24}(\mathbf{X} \otimes \mathbf{Y})$ denotes the usual Kronecker product of matrices, and $\mathbf{X} \oplus_K \mathbf{Y} := \mathbf{X} \otimes_K \mathbf{Y} + \mathbf{Y} \otimes_K \mathbf{X}$ denotes a symmetric Kronecker sum.

Proof. Let $\boldsymbol{\Lambda} \in \mathbb{R}^{r \times r \times p'}$ be a tensor of Lagrange multipliers and define the Lagrangian

$$L(\bar{\mathbf{T}}, \boldsymbol{\Lambda}) = \frac{1}{2} \sum_{s=1}^{N_s} \left\| \hat{\mathbf{Z}}_s - \hat{\mathbf{X}}_s(\bar{\mathbf{T}}\boldsymbol{\nu}_s) \hat{\mathbf{Y}}_s \right\|^2 + \langle \boldsymbol{\Lambda}, \bar{\mathbf{T}} \mp \bar{\mathbf{T}}^\top \rangle,$$

where, as before, $\bar{\mathbf{T}}^\top$ indicates transposition of the first two indices. Differentiating this expression, it follows that

$$\begin{aligned} dL(\bar{\mathbf{T}}, \boldsymbol{\Lambda}) &= - \sum_{s=1}^{N_s} \left\langle \hat{\mathbf{Z}}_s - \hat{\mathbf{X}}_s(\bar{\mathbf{T}}\boldsymbol{\nu}_s) \hat{\mathbf{Y}}_s, \hat{\mathbf{X}}_s(d\bar{\mathbf{T}}\boldsymbol{\nu}_s) \hat{\mathbf{Y}}_s \right\rangle \\ &\quad + \langle d\boldsymbol{\Lambda}, \bar{\mathbf{T}} \mp \bar{\mathbf{T}}^\top \rangle + \langle \boldsymbol{\Lambda}, d\bar{\mathbf{T}} \mp d\bar{\mathbf{T}}^\top \rangle \\ &= \left\langle d\bar{\mathbf{T}}, \boldsymbol{\Lambda} \mp \boldsymbol{\Lambda}^\top - \sum_{s=1}^{N_s} \hat{\mathbf{X}}_s^\top \left(\hat{\mathbf{Z}}_s - \hat{\mathbf{X}}_s(\bar{\mathbf{T}}\boldsymbol{\nu}_s) \hat{\mathbf{Y}}_s \right) \hat{\mathbf{Y}}_s^\top \otimes \boldsymbol{\nu}_s \right\rangle \\ &\quad + \left\langle d\hat{\boldsymbol{\Lambda}}, \bar{\mathbf{T}} \mp \bar{\mathbf{T}}^\top \right\rangle \\ &= \langle d\bar{\mathbf{T}}, \nabla_{\bar{\mathbf{T}}} L \rangle + \langle d\boldsymbol{\Lambda}, \nabla_{\boldsymbol{\Lambda}} L \rangle. \end{aligned}$$

Setting these gradients to zero yields the Euler–Lagrange equations for L ,

$$\mathbf{\Lambda} \mp \mathbf{\Lambda}^\top = \sum_{s=1}^{N_s} \hat{\mathbf{X}}_s^\top \left(\hat{\mathbf{Z}}_s - \hat{\mathbf{X}}_s(\bar{\mathbf{T}}\boldsymbol{\nu}_s) \hat{\mathbf{Y}}_s \right) \hat{\mathbf{Y}}_s^\top \otimes \boldsymbol{\nu}_s \quad (3.13a)$$

$$\bar{\mathbf{T}} \mp \bar{\mathbf{T}}^\top = \mathbf{0}. \quad (3.13b)$$

In particular, the Lagrange multiplier $\mathbf{\Lambda}$ can be eliminated by symmetrizing/anti-symmetrizing (3.13a), leading to

$$\sum_{s=1}^{N_s} \left[\hat{\mathbf{X}}_s^\top \left(\hat{\mathbf{Z}}_s - \hat{\mathbf{X}}_s(\bar{\mathbf{T}}\boldsymbol{\mu}_s) \hat{\mathbf{Y}}_s \right) \hat{\mathbf{Y}}_s^\top \right. \\ \left. \pm \hat{\mathbf{Y}}_s \left(\hat{\mathbf{Z}}_s - \hat{\mathbf{X}}_s(\bar{\mathbf{T}}\boldsymbol{\nu}_s) \hat{\mathbf{Y}}_s \right)^\top \hat{\mathbf{X}}_s \right] \otimes \boldsymbol{\nu}_s = \mathbf{0},$$

which, upon rearranging and applying (3.13b), yields the tensor equation

$$\sum_{s=1}^{N_s} \left(\hat{\mathbf{X}}_s^\top \hat{\mathbf{X}}_s(\bar{\mathbf{T}}\boldsymbol{\nu}_s) \hat{\mathbf{Y}}_s \hat{\mathbf{Y}}_s^\top + \hat{\mathbf{Y}}_s \hat{\mathbf{Y}}_s^\top(\bar{\mathbf{T}}\boldsymbol{\nu}_s) \hat{\mathbf{X}}_s^\top \hat{\mathbf{X}}_s \right) \otimes \boldsymbol{\nu}_s \\ = \sum_{s=1}^{N_s} \left(\hat{\mathbf{X}}_s^\top \hat{\mathbf{Z}}_s \hat{\mathbf{Y}}_s^\top \pm \hat{\mathbf{Y}}_s \hat{\mathbf{Z}}_s^\top \hat{\mathbf{X}}_s \right) \otimes \boldsymbol{\nu}_s.$$

This is a Sylvester equation in the first two indices of $\bar{\mathbf{T}}$, so applying the “vec trick” [40] yields a partial vectorization of dimension $r^2 \times p'$,

$$\sum_{s=1}^{N_s} \left(\hat{\mathbf{X}}_s^\top \hat{\mathbf{X}}_s \bar{\oplus}_K \hat{\mathbf{Y}}_s \hat{\mathbf{Y}}_s^\top \right) \text{cvec}_{12}(\bar{\mathbf{T}}) \boldsymbol{\nu}_s \boldsymbol{\nu}_s^\top = \sum_{s=1}^{N_s} \text{cvec}_{12} \left(\hat{\mathbf{X}}_s^\top \hat{\mathbf{Z}}_s \hat{\mathbf{Y}}_s^\top \pm \hat{\mathbf{Y}}_s \hat{\mathbf{Z}}_s^\top \hat{\mathbf{X}}_s \right) \boldsymbol{\nu}_s^\top.$$

Vectorizing again finally yields the equivalent matrix-vector system in the $r^2 p'$ unknowns of $\text{vec } \bar{\mathbf{T}} := \text{cvec}_{12}(\text{cvec}_{12} \bar{\mathbf{T}})$,

$$\sum_{s=1}^{N_s} \left[\boldsymbol{\nu}_s \boldsymbol{\nu}_s^\top \otimes_K \left(\hat{\mathbf{X}}_s^\top \hat{\mathbf{X}}_s \bar{\oplus}_K \hat{\mathbf{Y}}_s \hat{\mathbf{Y}}_s^\top \right) \right] \text{vec } \bar{\mathbf{T}} \\ = \sum_{s=1}^{N_s} \boldsymbol{\nu}_s \otimes_K \text{cvec}_{12} \left(\hat{\mathbf{X}}_s^\top \hat{\mathbf{Z}}_s \hat{\mathbf{Y}}_s^\top \pm \hat{\mathbf{Y}}_s \hat{\mathbf{Z}}_s^\top \hat{\mathbf{X}}_s \right),$$

since $\text{cvec}_{12}(\mathbf{uv}^\top) = \text{rvec}_{12}(\mathbf{vu}^\top) = \mathbf{v} \otimes_K \mathbf{u}$. \square

Solving (3.12) with $\mathbf{X}_s = \hat{\mathbf{J}}$, $\mathbf{Y}_s = \hat{\mathbf{Q}}_s$, $\mathbf{Z}_s = \dot{\hat{\mathbf{Q}}}_s$, and $\boldsymbol{\nu}_s = \boldsymbol{\mu}_s$ results in a symmetric tensor $\bar{\mathbf{T}}$ for defining the ROM (3.9). An example implementation for setting up and solving (3.12) is provided in Algorithm 3.1, which relies on a basic result about the exchange of Kronecker products and vectorization (see Lemma A.4).

3.3 Example: Wave equation

This section describes an application with canonical Hamiltonian structure to which Algorithm 3.1 may be applied. Consider the following initial boundary value problem for a wave on the bounded domain $\Omega \subset \mathbb{R}^d$, $d \in \{1, 2, 3\}$, with variable wave speed:

$$\begin{cases} \dot{y}(\mathbf{x}, t) = \nabla \cdot (c(\mathbf{x}, \boldsymbol{\mu})^2 \nabla y(\mathbf{x}, t)), & \mathbf{x} \in \Omega \times (0, t_f], \\ y(\mathbf{x}, t) = 0, & \mathbf{x} \in \partial\Omega \times (0, t_f], \\ y(\mathbf{x}, 0) = y_0(\mathbf{x}), & \mathbf{x} \in \Omega, \\ \dot{y}(\mathbf{x}, 0) = 0, & \mathbf{x} \in \Omega. \end{cases} \quad (3.14)$$

Algorithm 3.1 A NumPy/SciPy implementation for inferring a structured tensor $\bar{\mathbf{T}} = \pm \bar{\mathbf{T}}^\top$ using the linear system (3.12) derived in Theorem 3.1.

```

1  import numpy as np
2  import scipy.linalg as la
3
4  def infer_Tbar_with_symmetry(nus, Xs, Ys, Zs, symmetric: bool = True):
5      p, Ns = nus.shape
6      r, Nt, Ns = Ys.shape # or Zs.shape
7
8      XsTXs = np.einsum("kis,kjs->ijs", Xs, Xs)
9      YsYsT = np.einsum("iks,jks->ijs", Ys, Ys)
10     nusnusT = np.einsum("xs,ys->xys", nus, nus)
11
12     Btsr = np.einsum("xys,ijs,kls->xyijkl", nusnusT, XsTXs, YsYsT)
13     Btsr += Btsr.transpose(0, 1, 4, 5, 2, 3) # tensorized Kronecker sum
14     Bhat = Btsr.transpose(0, 2, 4, 1, 3, 5).reshape((r*r*p, r*r*p), order="C")
15
16     Ctsr = np.einsum("kis,kas,jas,xs->ijx", Xs, Zs, Ys, nus)
17     Ctsr += (1 if symmetric else -1) * Ctsr.transpose(1, 0, 2)
18     Chat = Ctsr.flatten(order="F")
19
20     vecT = la.solve(Bhat, Chat, assume_a="symmetric")
21     return vecT.reshape((r, r, p), order="F")

```

It is straightforward to check that the system (3.14) is Hamiltonian with the canonical variables $q = y$, $p = \dot{y}$ and Hamiltonian functional

$$H(q, p, \boldsymbol{\mu}) = \frac{1}{2} \int_{\Omega} p^2(\mathbf{x}) d\mathbf{x} + \frac{1}{2} \int_{\Omega} c^2(\mathbf{x}, \boldsymbol{\mu}) \|\nabla q(\mathbf{x})\|^2 d\mathbf{x}.$$

Suppose Ω can be partitioned into non-overlapping subdomains $\Omega = \cup_{i=1}^p \Omega_i$ representing different materials or media with wave speeds. Then $c^2 : \Omega \times \mathbb{R}^p \rightarrow \mathbb{R}$ is given by

$$c(\mathbf{x}, \boldsymbol{\mu})^2 = [\mathbf{x} \in \Omega_1] \mu_1^2 + [\mathbf{x} \in \Omega_2] \mu_2^2 + \dots + [\mathbf{x} \in \Omega_p] \mu_p^2, \quad \boldsymbol{\mu} = [\mu_1 \ \mu_2 \ \dots \ \mu_p]^\top.$$

With this choice, (3.14) is a locally linear, but globally nonlinear, Hamiltonian wave equation whose solution propagates with different speeds in each subdomain.

An appropriate FOM for (3.14) can be constructed via the Hamiltonian-preserving mixed finite element scheme from [49]. Given a triangulation $\Omega_h = \{K_i\}_{i=1}^{N_E}$ of Ω , define the spaces

$$\begin{aligned} W_h &:= \{w_h \in L^2(\Omega) : w_h|_K = P_k(K), \forall K \in \Omega_h\}, \\ V_h &:= \{\mathbf{v}_h \in H(\text{div}, \Omega) : \mathbf{v}_h|_K = RT_k(K), \forall K \in \Omega_h; \mathbf{v}_h|_{\partial\Omega} = 0\}, \end{aligned}$$

where $RT_k(K)$ is the order- k Raviart–Thomas space $[P_k(K)]^2 \oplus \mathbf{x}P_k(K)$ on element K and $P_k(K)$ denotes the space of polynomials of degree k on element K . The semi-discrete weak form can then be stated as follows: find $(\dot{q}_h, \dot{p}_h) \in W_h \times V_h$ such that

$$(\dot{q}_h, w_h)_{\Omega_h} = (p_h, w_h)_{\Omega_h} \quad \forall w_h \in W_h, \quad (3.15a)$$

$$(\dot{p}_h, w_h)_{\Omega_h} = (\nabla \cdot \boldsymbol{\sigma}_h, w_h)_{\Omega_h} \quad \forall w_h \in W_h, \quad (3.15b)$$

where $\boldsymbol{\sigma}_h \in V_h$ is a weak representation of $c^2 \nabla q$ and therefore satisfies

$$\left(\frac{1}{c(\boldsymbol{\mu})^2} \boldsymbol{\sigma}_h, \boldsymbol{\xi}_h \right)_{\Omega_h} + (q_h, \nabla \cdot \boldsymbol{\xi}_h)_{\Omega_h} = 0 \quad \forall \boldsymbol{\xi}_h \in V_h. \quad (3.15c)$$

The discrete Hamiltonian for this scheme is defined in analogy with the continuous case:

$$H_h(q_h, p_h) = \frac{1}{2}(p_h, p_h)_{\Omega_h} + \frac{1}{2} \left(\frac{1}{c(\boldsymbol{\mu})^2} \boldsymbol{\sigma}_h, \boldsymbol{\sigma}_h \right)_{\Omega_h}. \quad (3.16)$$

The mixed finite-element scheme (3.15) can be written in a matrix-vector form suitable for tensorization. It is shown in Appendix C that using \mathbf{M}_V and \mathbf{M}_W to denote the mass matrices associated with the spaces V_h and W_h , respectively, and collecting N degrees of freedom of finite element approximations of q_h and p_h into the vector $\mathbf{y} = [\mathbf{q}^\top \ \mathbf{p}^\top]^\top \in \mathbb{R}^{2N}$, the system formed from (3.15)–(3.15c) can be expressed as

$$\dot{\mathbf{y}} = \begin{bmatrix} \dot{\mathbf{q}} \\ \dot{\mathbf{p}} \end{bmatrix} = \begin{bmatrix} \mathbf{0} & \mathbf{I} \\ -\mathbf{I} & \mathbf{0} \end{bmatrix} \begin{bmatrix} \mathbf{M}_W^{-1} \mathbf{S}^\top \mathbf{M}_V(\boldsymbol{\mu})^{-1} \mathbf{S} & \mathbf{0} \\ \mathbf{0} & \mathbf{I} \end{bmatrix} \begin{bmatrix} \mathbf{q} \\ \mathbf{p} \end{bmatrix} = \mathbf{J} \mathbf{A}(\boldsymbol{\mu}) \mathbf{y}. \quad (3.17)$$

Importantly, the mass matrix $\mathbf{M}_V(\boldsymbol{\mu})$ depends affinely on $\boldsymbol{\mu}^{-2} = [\mu_1^{-2} \cdots \mu_p^{-2}]^\top \in \mathbb{R}^p$ and $\mathbf{A}(\boldsymbol{\mu}) = \text{blockdiag}(\mathbf{A}_1(\boldsymbol{\mu}), \mathbf{I})$ where $\mathbf{A}_1(\boldsymbol{\mu}) = \mathbf{M}_W^{-1} \mathbf{S}^\top \mathbf{M}_V(\boldsymbol{\mu})^{-1} \mathbf{S} \in \mathbb{R}^{N \times N}$. This is a canonical Hamiltonian system of the form (3.3) or, equivalently, (3.6), with respect to the joint mass matrix $\mathbf{M} = \text{blockdiag}(\mathbf{M}_W, \mathbf{M}_W)$ and the discrete Hamiltonian

$$H_h(\mathbf{y}, \boldsymbol{\mu}) = \frac{1}{2} \langle \mathbf{p}, \mathbf{p} \rangle_{\mathbf{M}_W} + \frac{1}{2} \langle \mathbf{q}, \mathbf{M}_W^{-1} \mathbf{S}^\top \mathbf{M}_V(\boldsymbol{\mu})^{-1} \mathbf{S} \mathbf{q} \rangle_{\mathbf{M}_W} = \frac{1}{2} \langle \mathbf{y}, \mathbf{A}(\boldsymbol{\mu}) \mathbf{y} \rangle_{\mathbf{M}},$$

where $\langle \mathbf{a}, \mathbf{b} \rangle_{\mathbf{M}_W} = \mathbf{a}^\top \mathbf{M}_W \mathbf{b}$ denotes the discrete inner product on W_h .

Because the affine parametric expansion of $\mathbf{M}_V(\boldsymbol{\mu})$ is in terms of $\boldsymbol{\mu}^{-2}$, it is reasonable to approximate the parametric dependence of $\mathbf{A}_1(\boldsymbol{\mu})$ as affine in the element-wise square $\boldsymbol{\mu}^2 = [\mu_1^2 \cdots \mu_p^2]^\top$ so that $\mathbf{A}_1(\boldsymbol{\mu}) \approx \mathbf{T}_1 \boldsymbol{\mu}^2$ for some constant tensor $\mathbf{T}_1 \in \mathbb{R}^{N \times N \times p}$. This also defines a tensor $\mathbf{T} \in \mathbb{R}^{2N \times 2N \times p}$ with $\mathbf{T} \boldsymbol{\mu}' \approx \mathbf{A}(\boldsymbol{\mu})$ with $\boldsymbol{\mu}' = [(\boldsymbol{\mu}^2)^\top, 1]^\top \in \mathbb{R}^{p+1}$ and entries

$$\mathbf{T}_{ijk} = [k \neq 1][i \leq N][j \leq N] (\mathbf{T}_1)_{ijk} + [k = 1][i > N][j = i],$$

which amounts to inserting the $N \times N$ identity alongside the approximation for $\mathbf{A}_1(\boldsymbol{\mu})$ through the last index of \mathbf{T} . It follows that the model $\dot{\mathbf{y}} = \mathbf{J}(\mathbf{T} \boldsymbol{\mu}') \mathbf{y}$ is an affine parametric approximation to the original wave equation (3.14) which retains its Hamiltonian structure, provided that $\mathbf{T}^* = \mathbf{T}$ is self-adjoint in its first two indices.

Remark 3.2. It is possible to express the Hamiltonian FEM scheme (3.15)–(3.16) in a way that exactly retains the affine parametric structure in (3.15c) from $\mathbf{M}_V(\boldsymbol{\mu})$. However, doing so requires simulating the intermediate variable $\boldsymbol{\sigma}_h$ and precludes the standard Hamiltonian expression $\dot{\mathbf{y}} = \mathbf{J} \nabla^M H(\mathbf{y})$. We have chosen to retain the approximate affine dependence $\mathbf{A}_1(\boldsymbol{\mu}) \approx \mathbf{T}_1 \boldsymbol{\mu}^2$ both for this reason and because it enables a demonstration of the proposed OpInf procedure in a case where the parametric dependence in the FOM is not fully affine.

Given an \mathbf{M} -orthonormal, \mathbf{J} -equivariant basis $\mathbf{U} \in \mathbb{R}^{2N \times 2r}$, Algorithm 3.1 can be applied to learn a reduced model

$$\dot{\hat{\mathbf{y}}} = \mathbf{J}(\bar{\mathbf{T}} \boldsymbol{\mu}') \hat{\mathbf{y}}, \quad \hat{\mathbf{y}}(0, \boldsymbol{\mu}) = \mathbf{U}^* \mathbf{y}_0(\boldsymbol{\mu}), \quad (3.18)$$

in terms of $\bar{\mathbf{T}} = \bar{\mathbf{T}}^\top$. Alternatively, since the parametric dependence of $\mathbf{A}(\boldsymbol{\mu})$ appears only in its upper-left block via $\mathbf{A}_1(\boldsymbol{\mu})$, one may construct a block-structured ROM

$$\dot{\hat{\mathbf{y}}} = \begin{bmatrix} \dot{\hat{\mathbf{q}}} \\ \dot{\hat{\mathbf{p}}} \end{bmatrix} = \begin{bmatrix} \mathbf{0} & \mathbf{I} \\ -\mathbf{I} & \mathbf{0} \end{bmatrix} \begin{bmatrix} \bar{\mathbf{T}}_1 \boldsymbol{\mu} & \mathbf{0} \\ \mathbf{0} & \bar{\mathbf{A}}_2 \end{bmatrix} \begin{bmatrix} \hat{\mathbf{q}} \\ \hat{\mathbf{p}} \end{bmatrix}, \quad \hat{\mathbf{y}}(0, \boldsymbol{\mu}) = \mathbf{U}^* \mathbf{y}_0(\boldsymbol{\mu}), \quad (3.19)$$

which requires a symmetric tensor $\bar{\mathbf{T}}_1 = \bar{\mathbf{T}}_1^\top$ inferred with Algorithm 3.1 and a symmetric matrix $\bar{\mathbf{A}}_2 = \bar{\mathbf{A}}_2^\top$ inferred with standard Hamiltonian OpInf [21, 47]. The numerical results reported in Section 4 use (3.19), but additional experiments were performed using the more general (3.18) without significant or qualitative differences to the outcomes.

4 Numerical results

This section applies tensor parametric OpInf to the parameterized heat and wave equation models introduced in earlier sections. Numerical experiments for each problem are conducted in one and two spatial dimensions, comparing both intrusive and non-intrusive ROMs. Accuracy is assessed using the relative L^2 -error in state approximations: if $\mathbf{Q}_s^{\text{FOM}}$ and $\mathbf{Q}_s^{\text{ROM}}$ are matrices of the FOM and ROM solutions, respectively, at the same parameter value and over N_t time instances with uniform time step $\delta t > 0$, the relative error is given by

$$RL^2(\mathbf{Q}_s^{\text{FOM}}, \mathbf{Q}_s^{\text{ROM}}) = \frac{\sqrt{\sum_s \|\mathbf{Q}_s^{\text{FOM}} - \mathbf{Q}_s^{\text{ROM}}\|_{\mathbf{M}}^2}}{\sqrt{\sum_s \|\mathbf{Q}_s^{\text{FOM}}\|_{\mathbf{M}}^2}}, \quad \|\mathbf{Q}\|_{\mathbf{M}}^2 = \text{trace}(\mathbf{Q}^{\top} \mathbf{M} \mathbf{Q}) N_t \delta t, \quad (4.1)$$

in which $\|\cdot\|_{\mathbf{M}}$ approximates the joint L^2 -norm over the spatial and temporal domains. For a given basis \mathbf{U} , the projection error is defined by replacing $\mathbf{Q}_s^{\text{ROM}}$ with $\mathbf{U}\mathbf{U}^* \mathbf{Q}_s^{\text{FOM}}$ in (4.1).

4.1 Heat equation

This section applies the structure-agnostic tensor parametric OpInf methods of Section 2 to the parameterized heat equation (2.13). An \mathbf{M} -orthonormal basis matrix $\mathbf{U} \in \mathbb{R}^{N \times r}$ is constructed through weighted proper orthogonal decomposition (POD) [5, 18, 48] as follows. Let $\mathbf{Y} = [\mathbf{R}\mathbf{Q}_1 \ \mathbf{R}\mathbf{Q}_2 \ \cdots \ \mathbf{R}\mathbf{Q}_{N_s}] \in \mathbb{R}^{N \times N_t N_s}$, where \mathbf{Q}_s is the FOM state snapshot matrix corresponding to training parameter value $\boldsymbol{\mu}_s$ and \mathbf{R} is the upper triangular Cholesky factor of the mass matrix, $\mathbf{R}^{\top} \mathbf{R} = \mathbf{M}$. For a fixed reduced dimension $r \ll N$, the basis matrix is then given by $\mathbf{U} = \mathbf{R}^{-1} \tilde{\mathbf{U}}_r$, where $\mathbf{Y} = \tilde{\mathbf{U}} \boldsymbol{\Sigma} \mathbf{V}^{\top}$ is the singular value decomposition (SVD) of \mathbf{Y} and $\tilde{\mathbf{U}}_r = \tilde{\mathbf{U}}_{:,r}$ denotes the first r columns of $\tilde{\mathbf{U}}$ (the r principal left singular vectors of \mathbf{Y}). It follows that $\mathbf{U}^* \mathbf{U} = \mathbf{U}^{\top} \mathbf{M} \mathbf{U} = \mathbf{U}^{\top} \mathbf{R}^{\top} \mathbf{R} \mathbf{U} = \tilde{\mathbf{U}}_r^{\top} \tilde{\mathbf{U}}_r = \mathbf{I}$, the desired orthonormality condition. Algorithm 2.1, which relies on solving the normal equations, and Algorithm 2.2, which employs an SVD-based least-squares solver, are applied to learn the tensor operator $\bar{\mathbf{T}} \approx \hat{\mathbf{T}}$ in (2.10). The results are denoted ‘‘OpInf (normal)’’ and ‘‘OpInf (SVD)’’, respectively.

4.1.1 One spatial dimension

First, consider the system (2.13) on the one-dimensional domain $\Omega = (0, 2\pi)$ with the parameterized heat conductivity coefficient

$$c(x, \boldsymbol{\mu}) = \left[x \in \left(0, \frac{2\pi}{3}\right) \right] \mu_1 + \left[x \in \left(\frac{2\pi}{3}, \frac{4\pi}{3}\right) \right] \mu_2 + \left[x \in \left(\frac{4\pi}{3}, 2\pi\right) \right] \mu_3, \quad \boldsymbol{\mu} \in \mathbb{R}^3.$$

The mesh Ω_h consists of uniform elements with a total of $N = 1001$ spatial degrees of freedom. To generate snapshot data for training, the FOM is integrated in time from $t_0 = 0$ using the Backward Euler method until final time $t_f = 8$, with step size $\Delta t = 0.008$, resulting in $N_t = 1001$ time points. The initial condition for this experiment is chosen to be

$$q(x, 0) = \exp(-(x - \pi)^2) \sin\left(\frac{x}{2}\right),$$

which is independent of $\boldsymbol{\mu}$. Snapshot data are generated over $N_s = 85$ training parameters and 15 test parameters uniformly sampled from the interval $(0.01, 1)^3$. The ROMs are also integrated in time using the Backward Euler method to generate reduced state approximations.

Figure 1 displays space-time contour plots of the FOM solution alongside ROM approximations of dimensionality $r = 6$, corresponding to a single test parameter. Each ROM yields acceptable errors, with the maximum relative error being around 6%. Additionally, both OpInf approaches yield nearly identical error profiles, suggesting that numerical conditioning is not an issue in this experiment. Figure 2 shows the relative error (4.1) in the ROM solutions, along with the projection error, as functions of the basis size r over all training and testing snapshots, respectively. Over the training snapshots, the two OpInf ROMs exhibit identical error profiles, closely matching that of the intrusive ROM up to $r = 21$, where they achieve an accuracy of 0.1%. For $r > 21$, the OpInf ROM errors saturate, while the error profile of the intrusive ROM continues to decrease. This behavior is expected, as OpInf ROMs generally do not pre-asymptotically

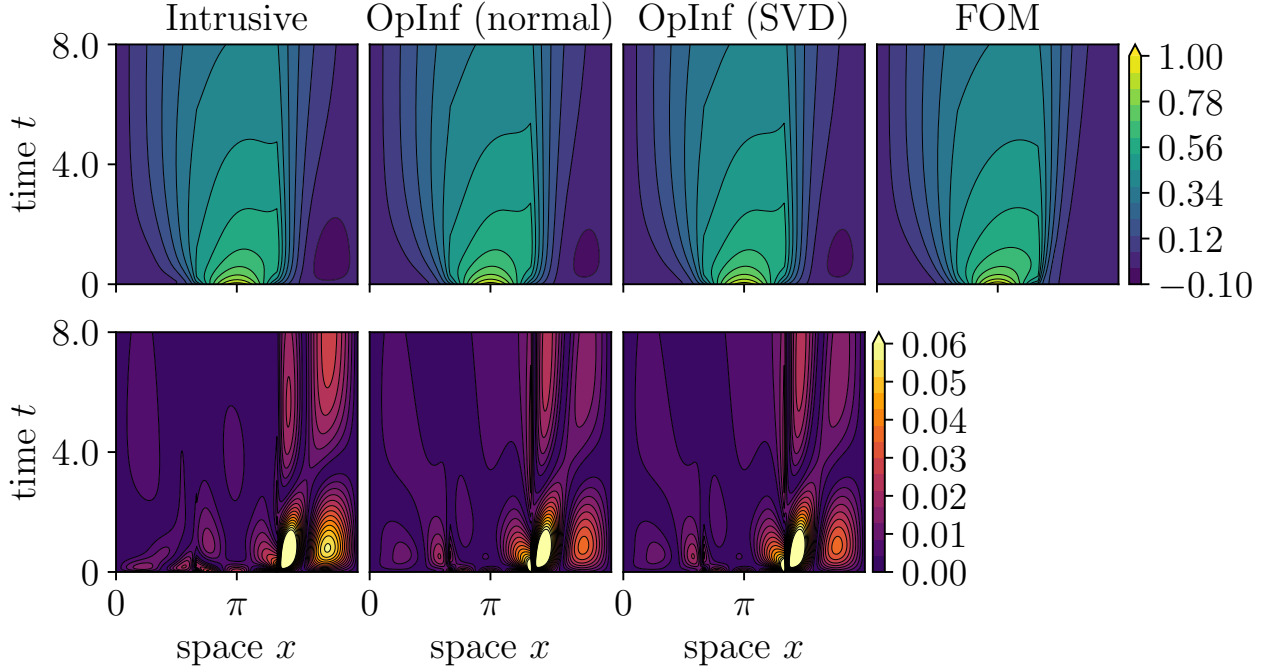


Figure 1: Top row: space-time contour plots of the FOM solution to the 1D heat equation at test parameter value $\boldsymbol{\mu} \approx [0.221, 0.523, 0.0354]^\top$, as well as ROM approximations with $r = 6$ basis vectors. Bottom row: absolute errors for each ROM.

recover the intrusive Galerkin ROM, and therefore closure error in the learned operator can degrade ROM accuracy in the finite-data regime [22, 34]. Similar error profiles are observed over the test snapshots with the exception of minor fluctuations at low numbers of modes. As seen in the reproductive case, the error profiles of the OpInf ROMs show a decreasing trend with a saturation of 0.1% beyond $r = 21$. This maintenance of advantageous error profiles across training and testing data demonstrates the generalizability of the learned OpInf ROMs to unseen parameter values.

4.1.2 Two spatial dimensions

Consider now the square two-dimensional spatial domain $\Omega = (0, 2\pi) \times (0, 2\pi)$. In this experiment, the parameterized heat conductivity coefficient is

$$c(\mathbf{x}, \boldsymbol{\mu}) = \left[\mathbf{x} \in (0, \pi)^2 \right] \mu_1 + \left[\mathbf{x} \in (\pi, 2\pi) \times (0, \pi) \right] \mu_2 + \left[\mathbf{x} \in (0, \pi) \times (\pi, 2\pi) \right] \mu_3 + \left[\mathbf{x} \in (\pi, 2\pi)^2 \right] \mu_4, \quad \boldsymbol{\mu} \in \mathbb{R}^4.$$

The mesh Ω_h is unstructured and contains 3138 simplicial elements, yielding $N = 1642$ spatial degrees of freedom. The terminal time is set to $t_f = 2$, with a time-step size of $\Delta t = 0.002$, resulting in $N_t = 1001$ points in time. As before, both the FOM and ROMs are time-integrated using the Backward Euler method, and the initial condition is defined to be

$$q(\mathbf{x}, 0) = \exp\left(- (x_1 - \pi)^2 - (x_2 - \pi)^2\right) \sin\left(\frac{x_1}{2}\right) \sin\left(\frac{x_2}{2}\right).$$

Training data are generated over $N_s = 43$ parameter values, while the test data spans 7 parameter values, all uniformly sampled from $(0.1, 1.0)^4$.

Figure 3 shows the time evolution of the FOM solution for a single test parameter, as well as the corresponding absolute errors in the ROM solutions with $r = 8$, at the terminal time. While the intrusive ROM exhibits the smallest deviation from the FOM solution, the errors in the OpInf ROMs are also small and comparable, with a maximum relative error of less than 0.8%. Finally, Figure 4 presents a comparison of the

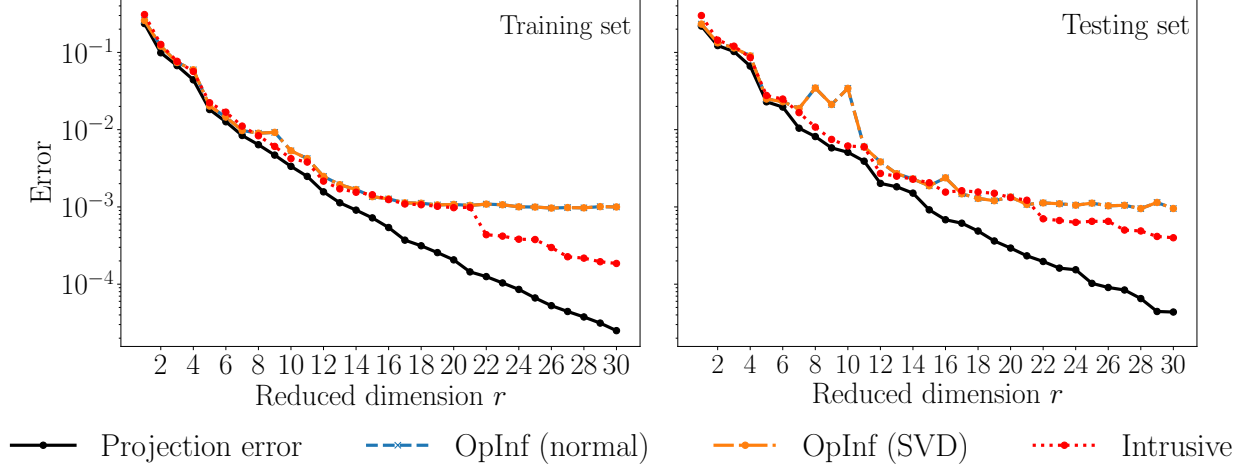


Figure 2: Relative L^2 error in the ROM generated solutions to the 1D heat system and the projection error of the FOM snapshot matrices as a function of reduced dimension r , over all training parameter values (left) and test parameter values (right).

relative L^2 -errors in the ROM solutions and the projection error, over the training and testing snapshots. For both training and test snapshots, the OpInf ROMs again produce identical error profiles that decay smoothly as r increases. In this case, the OpInf ROMs are observed to be slightly more accurate than the intrusive ROM, with no error saturation detected for $r \leq 30$. Additionally, the solution errors align very closely with the projection error, reaching approximately 0.2% at $r = 30$ over both the training and testing datasets.

4.2 Wave equation

The structure-preserving procedure from Section 3 is now applied to the parameterized wave equation initial boundary value problem (3.14) in one and two spatial dimensions. In each case, the basis matrix is constructed via PSD with the cotangent lift algorithm [36] as follows: Let $\mathbf{U}_W \in \mathbb{R}^{N \times r}$ be the \mathbf{M}_W -weighted POD basis of dimension r for $\mathbf{Y} = [\mathbf{RQ}_1 \cdots \mathbf{RQ}_{N_s} \mathbf{RP}_1 \cdots \mathbf{RP}_{N_s}] \in \mathbb{R}^{N \times 2N_t N_s}$, where $\mathbf{Q}_s, \mathbf{P}_s \in \mathbb{R}^{N \times N_t}$ are matrices containing the position and momentum FOM snapshots corresponding to training parameter $\boldsymbol{\mu}_s$, $s = 1, \dots, N_s$. Then the PSD basis is $\mathbf{U} = \text{blockdiag}(\mathbf{U}_W, \mathbf{U}_W) \in \mathbb{R}^{2N \times 2r}$, which is orthonormal with respect to $\mathbf{M} = \text{blockdiag}(\mathbf{M}_W, \mathbf{M}_W)$.

For comparison, two distinct approaches are employed to develop the non-intrusive ROMs. The structure-preserving approach (denoted ‘‘H-OpInf’’) infers the symmetric tensor $\bar{\mathbf{T}}_1 = \bar{\mathbf{T}}_1^\top$ in (3.19) using Algorithm 3.1 and the symmetric matrix $\bar{\mathbf{A}}_2 = \bar{\mathbf{A}}_2^\top$ through the standard Hamiltonian OpInf. Conversely, the structure-agnostic approach (‘‘OpInf’’) infers the two operators using Algorithm 2.1 and standard OpInf, respectively, without enforcing symmetry constraints. The performance of each ROM is assessed using two metrics: the relative error (4.1) (using the joint state variable $\mathbf{y} = [\mathbf{q}^\top \mathbf{p}^\top]^\top$) and the absolute error in the reduced Hamiltonian function as a function of time, $|\hat{H}(\hat{\mathbf{y}}(t), \boldsymbol{\mu}) - \hat{H}(\hat{\mathbf{y}}(0), \boldsymbol{\mu})|$.

4.2.1 One spatial dimension

In this experiment, the system (3.14) is considered on the domain $\Omega = (0, 2\pi)$ with the parameterized wave speed given by

$$c(x, \boldsymbol{\mu})^2 = \begin{aligned} & \left[x \in \left(0, \frac{\pi}{2}\right) \right] \mu_1^2 + \left[x \in \left(\frac{\pi}{2}, \pi\right) \right] \mu_2^2 \\ & + \left[x \in \left(\pi, \frac{3\pi}{2}\right) \right] \mu_3^2 + \left[x \in \left(\frac{3\pi}{2}, 2\pi\right) \right] \mu_4^2, \end{aligned} \quad \boldsymbol{\mu} \in \mathbb{R}^4.$$

The order of the space W_h is set to 0, while the order of V_h is chosen to be 1. The mesh Ω_h is composed of 1000 uniform elements with $N = 1000$ spatial degrees of freedom for the position and momentum variables.

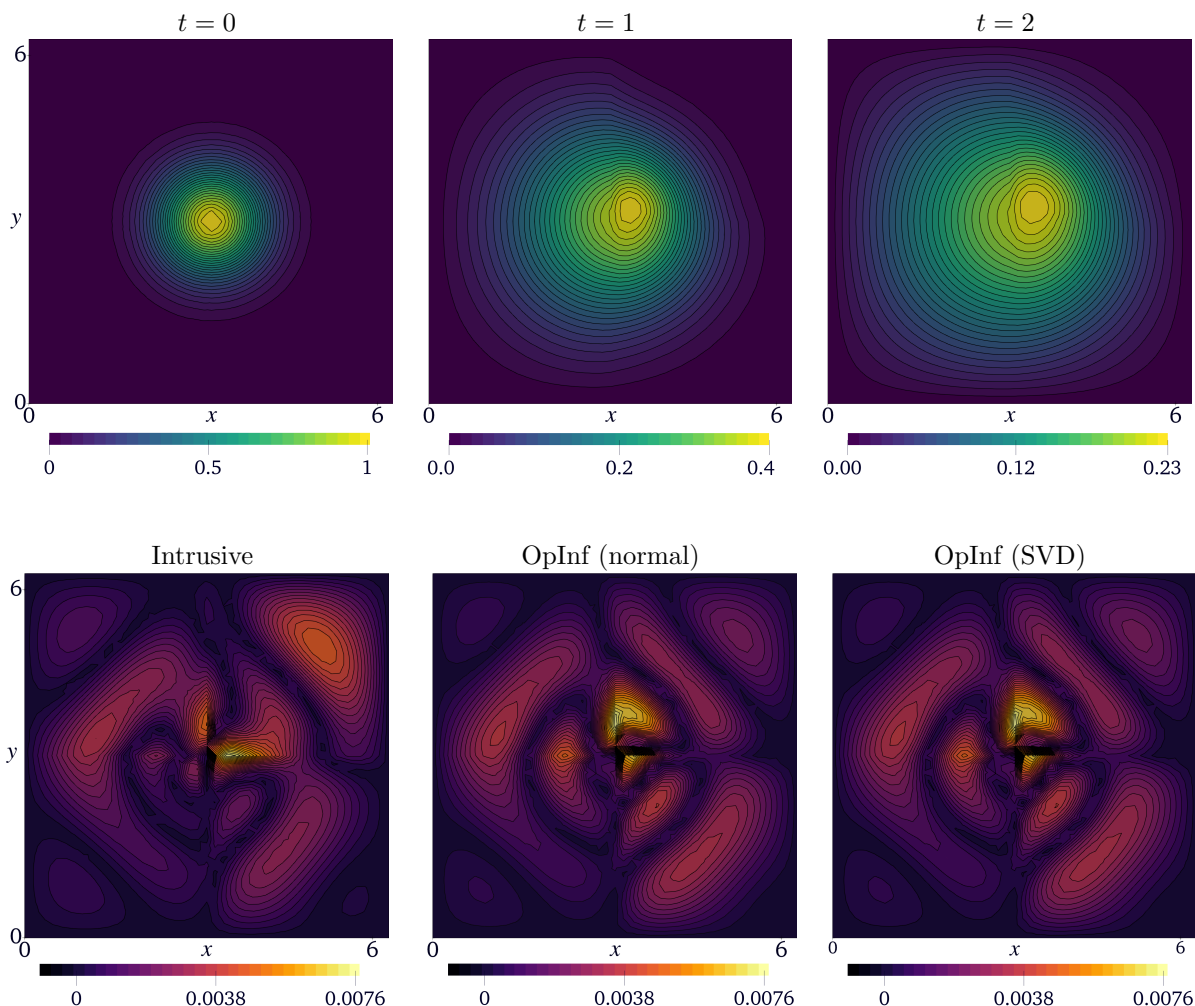


Figure 3: Top row: FOM solution to the 2D heat system at three different time instances for the testing parameter $\mu \approx [0.610, 0.3389, 0.571, 0.185]^T$. Bottom row: absolute error in the ROM approximations at the final time $t = 2$. Each ROM has dimension $r = 8$.

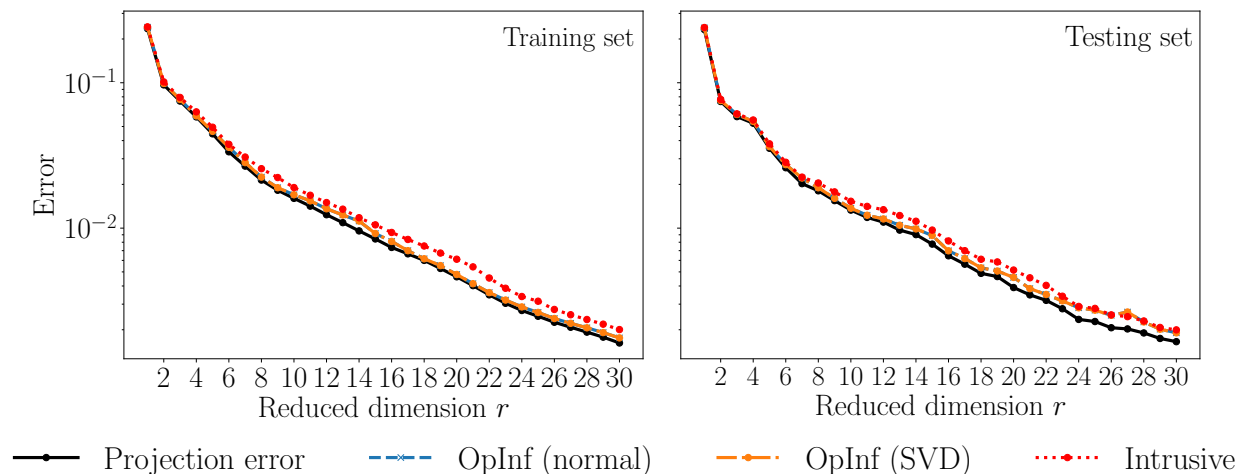


Figure 4: Relative L^2 error in the ROM generated solutions to the 2D heat system and the projection error of the FOM snapshot matrices as a function of reduced dimension r , over all training and test parameters.

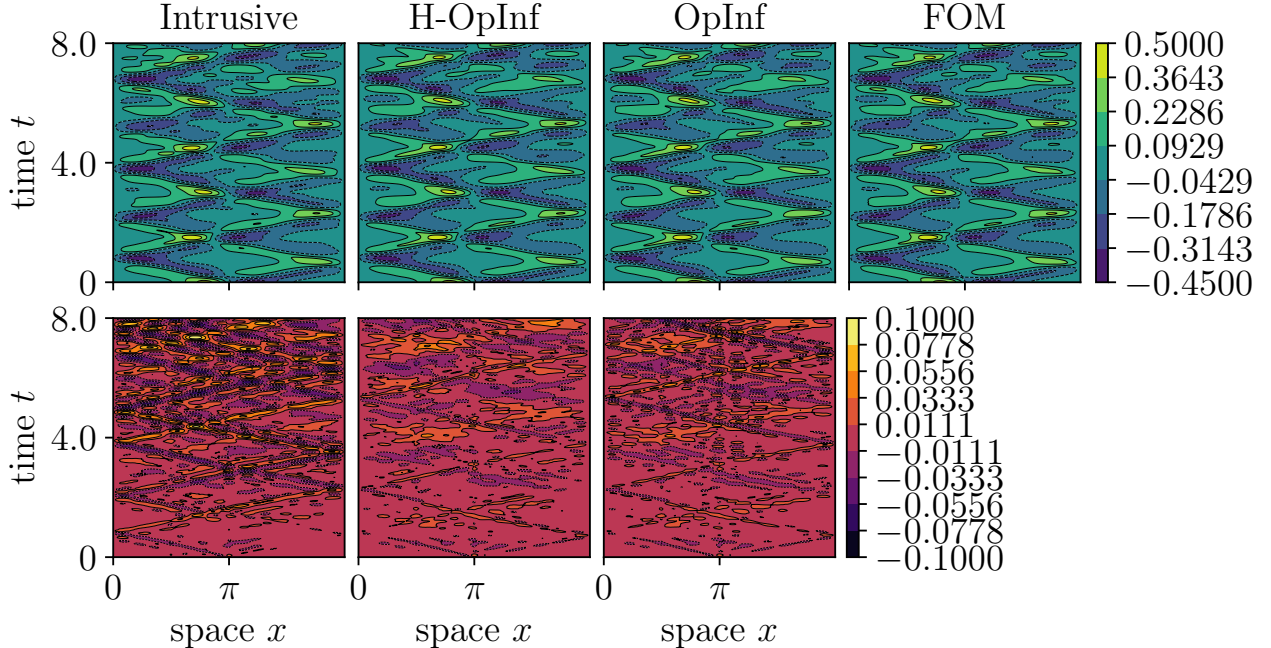


Figure 5: Top row: space-time contour plots of the FOM solution to the 1D wave equation with $\mu \approx [1.885, 1.232, 1.976, 2.340]^\top$, as well as ROM approximations with $2r = 12$. Bottom row: signed absolute errors for each ROM.

Snapshot data are generated by time-integrating the FOM (3.17) using the implicit midpoint rule,

$$\frac{\mathbf{y}^{n+1} - \mathbf{y}^n}{\Delta t} = \mathbf{J}\mathbf{A}(\mu)\mathbf{y}^{n+\frac{1}{2}}, \quad \mathbf{y}^0(x) = \mathbf{y}_0,$$

until terminal time $t_f = 8\pi$ with step-size $\Delta t = \frac{\pi}{100}$ for a total of $N_t = 801$ points in time. The initial condition is set to

$$y(x, 0) = \exp(-(x - \pi)^2) \sin x.$$

Snapshot data are obtained over 43 training parameter values and 7 test values, all uniformly sampled from the interval $(0.8, 2.4)^4$. The ROMs are also time-integrated using the implicit midpoint rule.

Figure 5 displays contour plots of the spacetime FOM solution alongside the corresponding ROM estimates for a reduced dimension of $r = 12$ at a single test parameter, as well as the signed absolute error in the ROM solutions. While all ROM approximations closely align with the FOM solution, the H-OpInf and OpInf ROMs achieve lower maximum relative errors of 5.8% and 6.6%, respectively, compared to the intrusive ROM's 9.7% error. Next, Figure 7 shows the relative errors in the ROM solutions and the projection error as functions of the reduced dimension $2r$ for all training and test snapshots, respectively. Both panels demonstrate a sustained decrease in ROM solution errors and projection errors as the number of modes increases, although the ROM errors plateau as $2r$ increases. The OpInf ROM exhibits slight instability for certain choices of $2r$ across both training and testing data. Figure 8, which shows the absolute error in the reduced Hamiltonian over time, highlights the key issue in the unconstrained OpInf ROM, namely that the reduced Hamiltonian is not conserved due to the loss of the symmetry structure. In contrast, both the intrusive ROM and the H-OpInf ROM conserve the reduced Hamiltonian to near machine precision. Over long integration times, the OpInf ROM gains energy erroneously and produces nonphysical and unreliable solutions.

To illustrate the effects of the erroneous energy gain by the OpInf ROM, consider a related experiment in which the training parameters are sampled from the exaggerated range $(0.8, 8)^4$. The terminal time for this experiment is changed to $t_f = 4\pi$, and the inference procedure is carried out as before, with the rest of the variables unchanged. ROMs of dimension $2r = 30$ are tested on a parameter within the training set.

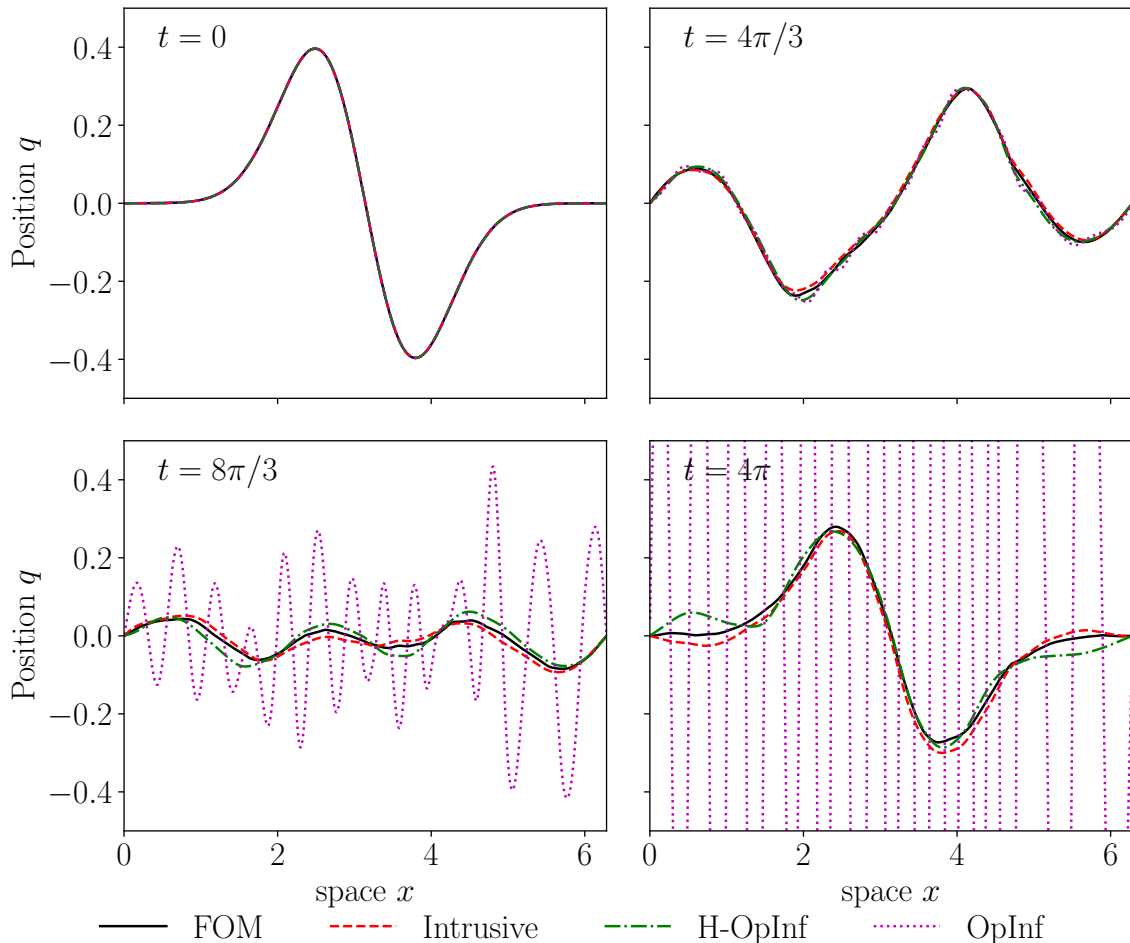


Figure 6: Emergence of non-physical oscillations and blow-up in an OpInf ROM solution to the 1D wave equation due to the lack of Hamiltonian structure preservation.

The results are displayed in Figure 6 and the second panel in Figure 8. Figure 6 displays the position variable \mathbf{q} at four different times, obtained from the FOM and all the ROMs. These plots reveal the emergence of nonphysical oscillations in the OpInf ROM's solution, which progressively amplify over time. In contrast, the solutions from the intrusive and the H-OpInf ROM remain approximately aligned with the FOM solution. The reason for the OpInf ROM's solution is made clear by the second panel of Figure 8, which shows a persistent gain in the energy of the OpInf ROM over time, an increase of approximately four orders of magnitude by terminal time. In contrast, the energy of both the intrusive and H-OpInf ROMs remains constant throughout, a consequence of their preserved symmetry structure.

4.2.2 Two spatial dimensions

The previous experiment is now repeated for the two-dimensional domain $\Omega = (0, \pi) \times (0, \pi)$. The wave speed is parameterized as

$$c(\mathbf{x}, \boldsymbol{\mu})^2 = \left[\mathbf{x} \in (0, \pi/2)^2 \right] \mu_1^2 + \left[\mathbf{x} \in (\pi/2, \pi) \times (0, \pi/2) \right] \mu_2^2 + \left[\mathbf{x} \in (0, \pi/2) \times (\pi/2, \pi) \right] \mu_3^2 + \left[\mathbf{x} \in (\pi/2, \pi)^2 \right] \mu_4^2, \quad \boldsymbol{\mu} \in \mathbb{R}^4.$$

For this experiment, the order k of the finite-element spaces W_h and V_h is set to 2. Using an unstructured mesh of 512 elements, this configuration results in $N = 3072$ spatial degrees of freedom for both the position

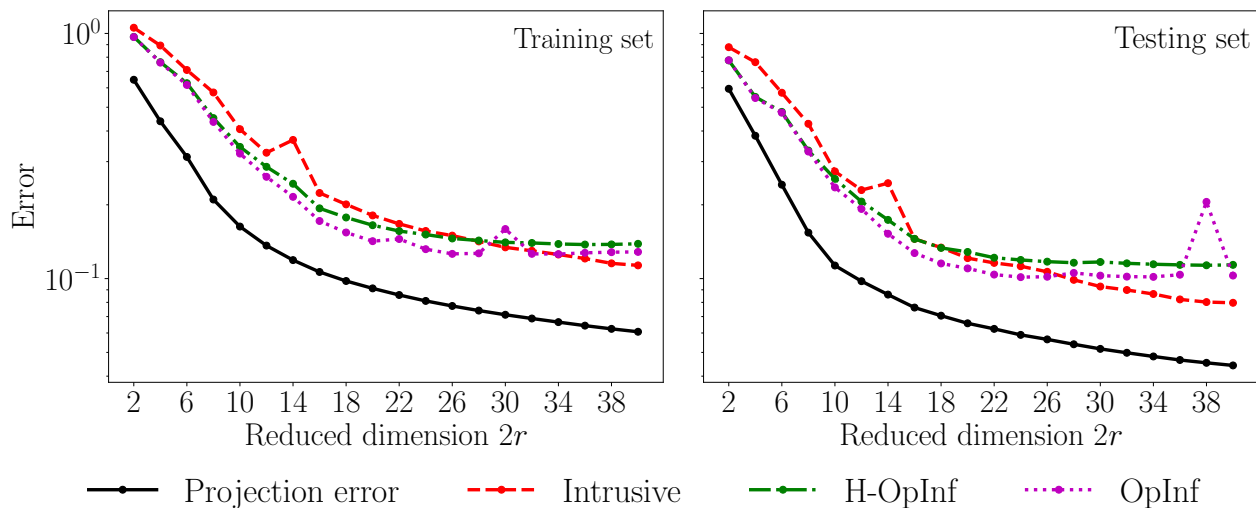


Figure 7: Relative L^2 error in the ROM generated solutions to the 1D wave system and the projection error of the FOM snapshot matrices as a function of reduced dimension r , over all training and test parameters.

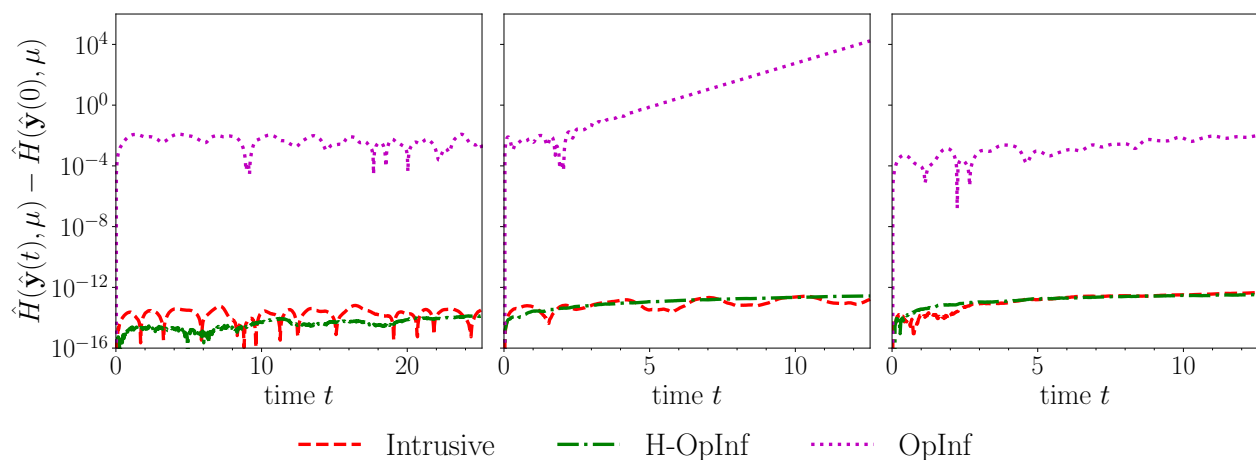


Figure 8: Absolute error in the reduced Hamiltonian versus time, for the ROM solutions to the wave equation displayed in Figure 5 (left), Figure 6 (middle), and Figure 9 (right).

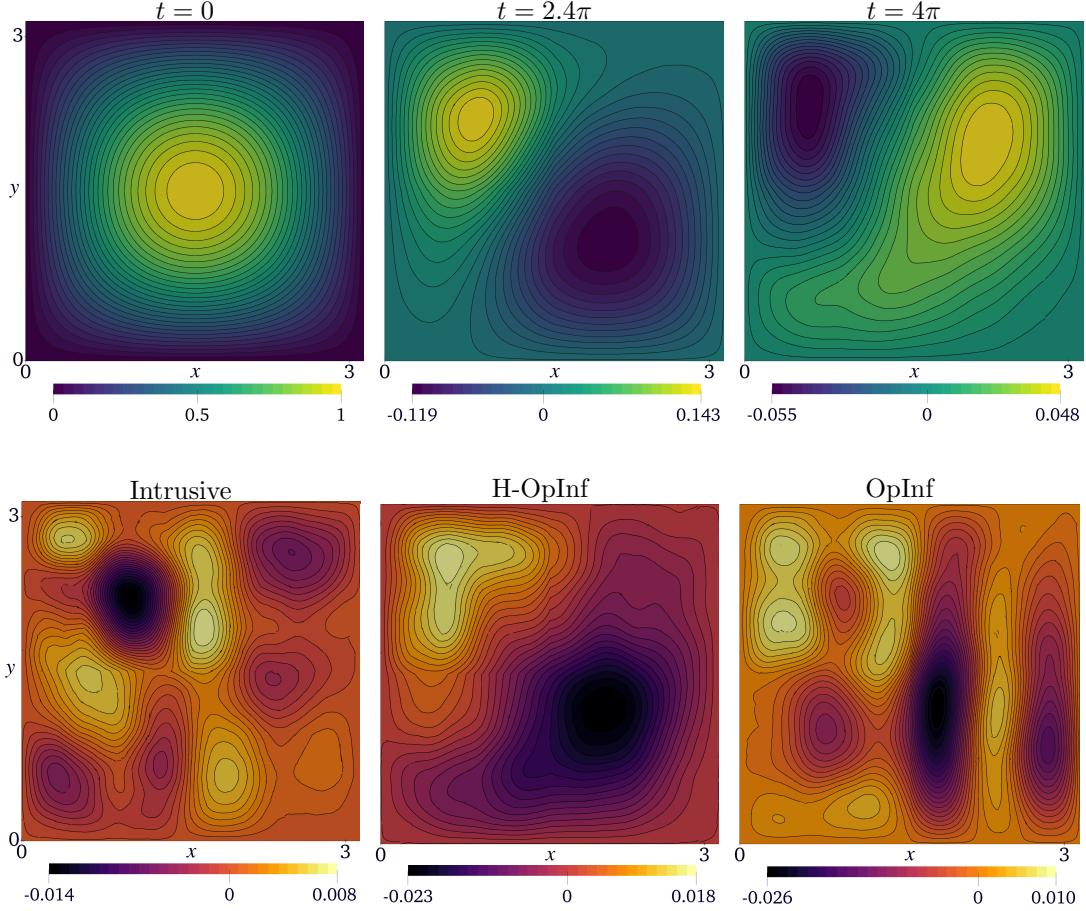


Figure 9: Top row: FOM solution to the 2D wave system at different times. Bottom row: signed error in the ROM approximations at $t = 4\pi$. Here, $2r = 18$ and $\boldsymbol{\mu} = [1.722, 2.287, 1.310, 1.868]^\top$.

and momentum variables. A terminal time of $t_f = 4\pi$ with $\Delta t = \frac{\pi}{500}$ yields $N_t = 501$ points in time. The initial condition is given by

$$y(\mathbf{x}, 0) = \exp(-0.01(x_1 - \pi) - 0.01(x_2 - \pi)) \sin(x_1) \sin(x_2)$$

A total of $N_s = 18$ training and 7 test parameters are sampled from the same space as in the previous experiment. Figure 9 depicts the FOM-computed position variable \mathbf{q} at three different times for a single test parameter, along with the corresponding signed errors in the ROM-computed \mathbf{q} at terminal time, with $2r = 18$. It is clear from these that the intrusive ROM achieves the highest accuracy at terminal time, with a maximum relative error of approximately 1.4%, whereas the OpInf ROM yields the largest error, around 2.6%. The last frame of Figure 8, which shows the evolution of the absolute error in the reduced Hamiltonian over time, reveals that the H-OpInf and intrusive ROMs conserve the reduced Hamiltonian to machine precision, while the OpInf ROM exhibits significant error with a persistent energy gain.

Finally, Figure 10 shows the relative error in the three ROM solutions over the training and testing sets, together with the respective projection errors. The error profiles show similar trends as those in the one-dimensional experiment. However the saturation of the ROM solution errors is not observed for number of modes up to 40. The OpInf ROM is observed to be noticeably unstable over the test snapshots, for several values $2r$. Contrarily, the intrusive and H-OpInf ROMs yield stable error trends that are consistent across the training and testing sets.

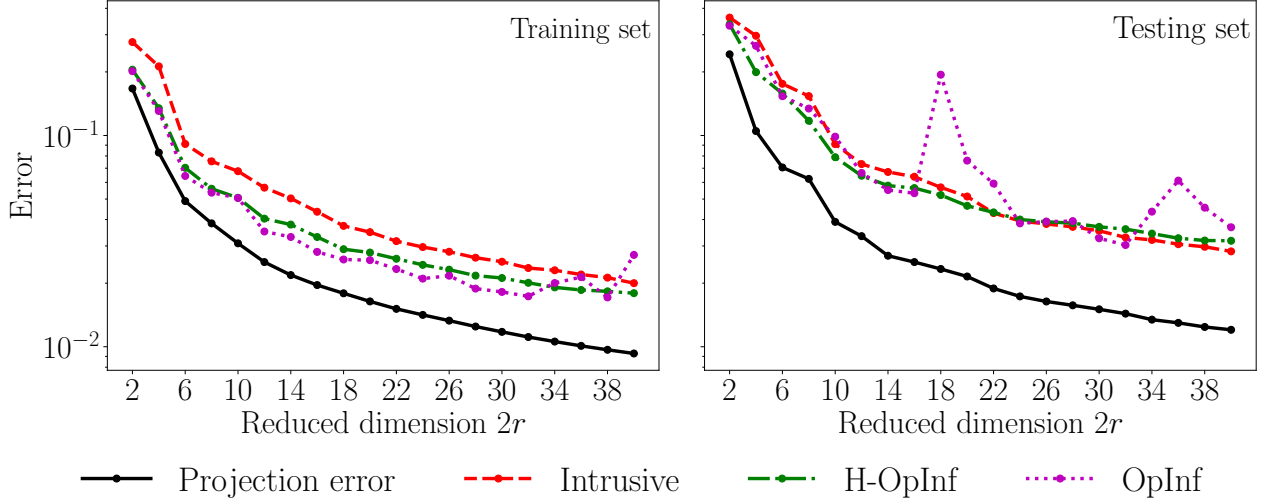


Figure 10: Relative L^2 error in the ROM generated solutions to the 2D wave system and the projection error of the FOM snapshot matrices as a function of reduced dimension r , over all training and test parameters.

5 Conclusion

This paper presents a novel, tensor-based operator inference procedure for non-intrusively learning reduced-order models corresponding to parametric systems of semi-discrete PDEs. In its most basic form, the proposed method serves as a compact, easy-to-implement replacement for the state-linear component of existing parametric OpInf strategies. Additionally, it is shown that the advantages of this formulation enable an extension to the inference of operators with additional structure information, such as partial symmetries, which appear in the contexts of Hamiltonian systems and gradient flows. Applications to a heat equation with variable diffusion coefficient and a Hamiltonian wave equation with variable wave speed are presented, where the proposed OpInf leads to structure-preserving ROMs which are energy-conserving and symplectic in the Hamiltonian case as required.

The structure-preserving inference procedure of Section 3, specifically in Theorem 3.1 and Algorithm 3.1, is based on a linear solve of the normal equations corresponding to a particular minimization problem. It would be interesting to consider future extensions of this approach which avoid the potential for ill-conditioning, i.e., to develop an extension of Algorithm 2.2 to the structure-preserving setting. This may have the secondary benefit of removing the need for a large, memory-intensive intermediate tensors that are required for symmetry enforcement in the current approach, as well as the potential for greater parallelism and preconditioning to improve convergence. Future work will also consider incorporating additional constraints on the learned operators beyond symmetry, as well as accounting for nonlinear terms arising from non-quadratic Hamiltonians, i.e., when $f \neq 0$ in (3.4)–(3.5).

Acknowledgments

Support for this work was received through the U.S. Department of Energy, Office of Science, Office of Advanced Scientific Computing Research, Mathematical Multifaceted Integrated Capability Centers (MMICCS) program, under Field Work Proposal 22025291 and the Multifaceted Mathematics for Predictive Digital Twins (M2dt) project. A.G. and S.A.M. acknowledge additional support from the John von Neumann Fellowship, a position sponsored by Sandia National Laboratories in conjunction with the Applied Mathematics Program of the U.S. Department of Energy Office of Advanced Scientific Computing Research. Sandia National Laboratories is a multimission laboratory managed and operated by National Technology & Engineering Solutions of Sandia, LLC, a wholly owned subsidiary of Honeywell International Inc., for the U.S. Department of Energy's National Nuclear Security Administration under contract DE-NA0003525. This paper describes objective technical results and analysis. Any subjective views or opinions that might

be expressed in the paper do not necessarily represent the views of the U.S. Department of Energy or the United States Government.

Appendix A Tensor algebra lemmata

This appendix lists tensor algebra conventions and proves minor results that are used in Sections 2 and 3.

Definition A.1 (Frobenius inner product). Consider the Cartesian product $X = \mathbb{R}^{N_1 \times \dots \times N_n}$. For order- n tensors $\mathbf{A}, \mathbf{B} \in X$ with entries A_{i_1, \dots, i_n} and B_{i_1, \dots, i_n} , respectively, the *Frobenius inner product* $\langle \cdot, \cdot \rangle : X \times X \rightarrow \mathbb{R}$ is the bilinear operator

$$\langle \mathbf{A}, \mathbf{B} \rangle = \sum_{i_1=1}^{N_1} \sum_{i_2=1}^{N_2} \dots \sum_{i_n=1}^{N_n} A_{i_1, \dots, i_n} B_{i_1, \dots, i_n}.$$

Lemma A.1 (Properties of the Frobenius inner product). Let $\langle \cdot, \cdot \rangle$ denote the Frobenius inner product, with the domain inferred from the context. For $\mathbf{A} \in \mathbb{R}^{\ell \times m}$, $\mathbf{B} \in \mathbb{R}^{m \times n}$, and $\mathbf{C} \in \mathbb{R}^{\ell \times n}$,

$$\langle \mathbf{AB}, \mathbf{C} \rangle = \langle \mathbf{A}, \mathbf{CB}^\top \rangle.$$

Moreover, if $\mathbf{T} \in \mathbb{R}^{m \times n \times p'}$ and $\boldsymbol{\nu} \in \mathbb{R}^{p'}$, then

$$\langle \mathbf{T}\boldsymbol{\nu}, \mathbf{B} \rangle = \langle \mathbf{T}, \mathbf{B} \otimes \boldsymbol{\nu} \rangle,$$

where \otimes denotes the outer product.

Proof. Denoting the entries of \mathbf{A} , \mathbf{B} , and \mathbf{C} with A_{ij} , B_{ij} , and C_{ij} , respectively,

$$\langle \mathbf{AB}, \mathbf{C} \rangle = \sum_{i=1}^{\ell} \sum_{j=1}^n \left(\sum_{k=1}^m A_{ik} B_{kj} \right) C_{ij} = \sum_{i=1}^{\ell} \sum_{k=1}^m A_{ik} \left(\sum_{j=1}^n C_{ij} B_{kj} \right) = \langle \mathbf{A}, \mathbf{CB}^\top \rangle.$$

Next, denoting the entries of \mathbf{T} with T_{ijk} and the entries of $\boldsymbol{\nu}$ with ν_i ,

$$\langle \mathbf{T}\boldsymbol{\nu}, \mathbf{B} \rangle = \sum_{k=1}^m \sum_{j=1}^n \left(\sum_{i=1}^{p'} T_{kji} \nu_i \right) B_{kj} = \sum_{k=1}^m \sum_{j=1}^n \sum_{i=1}^{p'} T_{kji} (B_{kj} \nu_i) = \langle \mathbf{T}, \mathbf{B} \otimes \boldsymbol{\nu} \rangle.$$

□

Definition A.2 (Tensor contraction). Let

$$\mathbf{A} \in \mathbb{R}^{N_1 \times \dots \times N_{n-2} \times X \times Y} \quad \text{and} \quad \mathbf{B} \in \mathbb{R}^{Y \times X \times M_3 \times \dots \times M_m}$$

with entries $A_{i_1, \dots, i_{n-2}, i_x, i_y}$ and $B_{k_y, k_x, k_3, \dots, k_m}$, respectively. The contraction

$$\mathbf{A} : \mathbf{B} \in \mathbb{R}^{N_1 \times \dots \times N_{n-2} \times M_3 \times \dots \times M_m}$$

is the tensor of order $N + M - 2$ with entries

$$(\mathbf{A} : \mathbf{B})_{i_1, \dots, i_{n-2}, k_3, \dots, k_m} = \sum_{x=1}^X \sum_{y=1}^Y A_{i_1, \dots, i_{n-2}, x, y} B_{y, x, k_3, \dots, k_m}.$$

Lemma A.2 (Outer product and contraction). For $\mathbf{T} \in \mathbb{R}^{r \times r \times p'}$, $\mathbf{B} \in \mathbb{R}^{r \times r}$, and $\boldsymbol{\nu} \in \mathbb{R}^{p'}$,

$$(\mathbf{T}\boldsymbol{\nu})\mathbf{B} \otimes \boldsymbol{\nu} = \mathbf{T} : (\boldsymbol{\nu} \otimes \mathbf{B} \otimes \boldsymbol{\nu}),$$

where $:$ is the contraction operator of Definition A.2.

Proof. Let T_{ijk} , B_{ij} , and ν_i denote the entries of \mathbf{T} , \mathbf{B} , and $\boldsymbol{\nu}$, respectively. Working componentwise,

$$((\mathbf{T}\boldsymbol{\nu})\mathbf{B} \otimes \boldsymbol{\nu})_{ijk} = \sum_{a=1}^r (\mathbf{T}\boldsymbol{\nu})_{ia} (\mathbf{B} \otimes \boldsymbol{\nu})_{ajk} = \sum_{a=1}^r \sum_{b=1}^{p'} T_{iab} \nu_b B_{aj} \nu_k.$$

On the other hand,

$$(\mathbf{T} : (\boldsymbol{\nu} \otimes \mathbf{B} \otimes \boldsymbol{\nu}))_{ijk} = \sum_{a=1}^r \sum_{b=1}^{p'} T_{iab} (\boldsymbol{\nu} \otimes \mathbf{B} \otimes \boldsymbol{\nu})_{bajk} = \sum_{a=1}^r \sum_{b=1}^{p'} T_{iab} \nu_b B_{aj} \nu_k.$$

□

Lemma A.3 (Vectorization and contraction). *For tensors $\mathbf{T} \in \mathbb{R}^{r \times r \times p'}$ and $\mathbf{X} \in \mathbb{R}^{p' \times r \times r \times p'}$,*

$$\text{cvec}_{23}(\mathbf{T} : \mathbf{X}) = (\text{cvec}_{23} \mathbf{T})(\text{rvec}_{12} \text{cvec}_{34} \mathbf{X}),$$

where $:$ is the contraction operator of Definition A.2.

Proof. Let T_{ijk} and X_{ijkl} denote the entries of \mathbf{T} and \mathbf{X} , respectively. Working componentwise,

$$(\text{cvec}_{23}(\mathbf{T} : \mathbf{X}))_{i,(k-1)r+j} = (\mathbf{T} : \mathbf{X})_{ijk} = \sum_{a=1}^r \sum_{b=1}^{p'} T_{iab} X_{bajk}$$

for each $1 \leq i, j \leq r$ and $1 \leq k \leq p'$. On the other hand, for $1 \leq a \leq r$ and $1 \leq b \leq p'$,

$$\begin{aligned} (\text{cvec}_{23} \mathbf{T})_{i,(b-1)r+a} &= T_{iab}, \\ (\text{rvec}_{12} \text{cvec}_{34} \mathbf{X})_{(b-1)r+a,(k-1)r+j} &= (\text{cvec}_{34} \mathbf{X})_{b,a,(k-1)r+j} = X_{bajk}. \end{aligned}$$

Hence, the $(i, (k-1)r+j)$ -th entry of $(\text{cvec}_{23} \mathbf{T})(\text{rvec}_{12} \text{cvec}_{34} \mathbf{X})$ is given by

$$\sum_{a=1}^r \sum_{b=1}^{p'} (\text{cvec}_{23} \mathbf{T})_{i,(b-1)r+a} (\text{rvec}_{12} \text{cvec}_{34} \mathbf{X})_{(b-1)r+a,(k-1)r+j} = \sum_{a=1}^r \sum_{b=1}^{p'} T_{iab} X_{bajk},$$

which completes the proof. □

Lemma A.4 (Iterated vectorization and the Kronecker product). *Let $\mathbf{A}, \mathbf{B}, \mathbf{C}$ be matrices potentially with different dimensions, and let $\text{rvec}_{135} = \text{rvec}_{13} \text{rvec}_{35}$. Then,*

$$\mathbf{A} \otimes_K (\mathbf{B} \otimes_K \mathbf{C}) = \text{rvec}_{135} \text{rvec}_{246} (\mathbf{A} \otimes \mathbf{B} \otimes \mathbf{C}).$$

Proof. By the definition of the Kronecker product, it follows that

$$\begin{aligned} \mathbf{A} \otimes_K (\mathbf{B} \otimes_K \mathbf{C}) &= \text{rvec}_{13} \text{rvec}_{24} (\mathbf{A} \otimes \text{rvec}_{13} \text{rvec}_{24} (\mathbf{B} \otimes \mathbf{C})) \\ &= \text{rvec}_{13} \text{rvec}_{24} (\text{rvec}_{35} \text{rvec}_{46} (\mathbf{A} \otimes \mathbf{B} \otimes \mathbf{C})) \\ &= \text{rvec}_{13} \text{rvec}_{35} \text{rvec}_{24} \text{rvec}_{46} (\mathbf{A} \otimes \mathbf{B} \otimes \mathbf{C}), \end{aligned}$$

which immediately implies the conclusion. □

Appendix B Adjoint and gradients

This appendix briefly outlines the relationship between adjoints and gradients with respect to different inner products.

Lemma B.1 (Weighted adjoint). *Suppose $\mathbf{A} \in \mathbb{R}^{N \times N}$ and $\mathbf{x}, \mathbf{y} \in \mathbb{R}^N$. Then the adjoint \mathbf{A}^* of \mathbf{A} with respect to the inner product $\langle \mathbf{x}, \mathbf{y} \rangle_{\mathbf{M}} = \mathbf{x}^\top \mathbf{M} \mathbf{y}$ defined by the symmetric and positive definite matrix $\mathbf{M} \in \mathbb{R}^{N \times N}$ is $\mathbf{A}^* = \mathbf{M}^{-1} \mathbf{A}^\top \mathbf{M}$.*

Proof. Observe that

$$\langle \mathbf{A}\mathbf{x}, \mathbf{y} \rangle_{\mathbf{M}} = \mathbf{x}^\top \mathbf{A}^\top \mathbf{M} \mathbf{y} = \mathbf{x}^\top \mathbf{M} (\mathbf{M}^{-1} \mathbf{A}^\top \mathbf{M}) \mathbf{y} = \langle \mathbf{x}, (\mathbf{M}^{-1} \mathbf{A}^\top \mathbf{M}) \mathbf{y} \rangle_{\mathbf{M}}.$$

□

The adjoint of a non-square matrix $\mathbf{U} \in \mathbb{R}^{N \times r}$ is only slightly more delicate, requiring weighted inner products on both \mathbb{R}^N and \mathbb{R}^r .

Lemma B.2 (Weighted non-square adjoint). *Let $\mathbf{U} \in \mathbb{R}^{N \times r}$, $\hat{\mathbf{x}} \in \mathbb{R}^r$, $\mathbf{y} \in \mathbb{R}^N$, and suppose $\mathbf{M} \in \mathbb{R}^{N \times N}$ and $\hat{\mathbf{M}} \in \mathbb{R}^{r \times r}$ are symmetric positive definite. Then the adjoint of \mathbf{U} with respect to the \mathbf{M} and $\hat{\mathbf{M}}$ inner products is $\mathbf{U}^* = \hat{\mathbf{M}}^{-1} \mathbf{U}^\top \mathbf{M}$.*

Proof. Similar to before, observe that

$$\langle \mathbf{U} \hat{\mathbf{x}}, \mathbf{y} \rangle_{\mathbf{M}} = \hat{\mathbf{x}}^\top \mathbf{U}^\top \mathbf{M} \mathbf{y} = \hat{\mathbf{x}}^\top \hat{\mathbf{M}} (\hat{\mathbf{M}}^{-1} \mathbf{U}^\top \mathbf{M}) \mathbf{y} = \langle \hat{\mathbf{x}}, (\hat{\mathbf{M}}^{-1} \mathbf{U}^\top \mathbf{M}) \mathbf{y} \rangle_{\hat{\mathbf{M}}}.$$

□

The previous results connect the \mathbf{M} -adjoint to the Euclidean adjoint. The next result establishes the same connection for the gradient operator on scalar functions.

Lemma B.3 (Weighted gradient). *Let $f : \mathbb{R}^N \rightarrow \mathbb{R}$ be a differentiable function and $\mathbf{M} \in \mathbb{R}^{N \times N}$ be a symmetric positive definite matrix. Then the gradient of f with respect to the \mathbf{M} -weighted inner product is $\nabla^{\mathbf{M}} f = \mathbf{M}^{-1} \nabla f$.*

Proof. For any $\mathbf{x}, \mathbf{v} \in \mathbb{R}^N$, it follows from Taylor's theorem that

$$df|_{\mathbf{x}}(\mathbf{v}) = \mathbf{v}^\top \nabla f(\mathbf{x}) = \mathbf{v}^\top \mathbf{M} \mathbf{M}^{-1} \nabla f(\mathbf{x}) = \langle \mathbf{v}, \mathbf{M}^{-1} \nabla f(\mathbf{x}) \rangle.$$

Since \mathbf{v} is arbitrary, this implies that $\nabla f = \mathbf{M} \nabla^{\mathbf{M}} f$ and the conclusion follows. □

The final result shows why affine-parametric state matrices can be assumed to be self-adjoint in the Hamiltonian systems context.

Lemma B.4 (Self-adjointness in quadratic functionals). *Let $\mathbf{A}, \mathbf{M} \in \mathbb{R}^{N \times N}$ and assume that \mathbf{M} is symmetric and positive definite. Only the self-adjoint part of \mathbf{A} contributes to the value of the quadratic functional $H : \mathbb{R}^N \rightarrow \mathbb{R}$ given by $H(\mathbf{y}) = \mathbf{y}^* \mathbf{A} \mathbf{y} = \mathbf{y}^\top \mathbf{M} \mathbf{A} \mathbf{y}$. Specifically, $H(\mathbf{y})$ is proportional to $\mathbf{y}^* (\mathbf{A} + \mathbf{A}^*) \mathbf{y}$.*

Proof. Decomposing \mathbf{A} into adjoint and skew-adjoint parts,

$$H(\mathbf{y}) = \frac{1}{2} \mathbf{y}^* (\mathbf{A} + \mathbf{A}^*) \mathbf{y} + \frac{1}{2} \mathbf{y}^* (\mathbf{A} - \mathbf{A}^*) \mathbf{y}.$$

Because \mathbf{M} is symmetric,

$$\mathbf{y}^* \mathbf{A} \mathbf{y} = (\mathbf{y}^\top \mathbf{M} \mathbf{A} \mathbf{y})^\top = \mathbf{y}^\top \mathbf{M} \mathbf{M}^{-1} \mathbf{A}^\top \mathbf{M} \mathbf{y} = \mathbf{y}^* \mathbf{A}^* \mathbf{y},$$

and hence $\mathbf{y}^* (\mathbf{A} - \mathbf{A}^*) \mathbf{y} = 0$. □

Appendix C Wave equation finite element model

This appendix derives the matrix-vector representations of the full-order finite element discretization used in Section 4.2 for the parameterized wave equation (3.14). Suppose $\{\phi_i\}_{i=1}^{N_W}$ and $\{\psi_i\}_{i=1}^{N_V}$ are basis functions for the spaces W_h and V_h , respectively, and let \mathbf{q}, \mathbf{p} , and $\boldsymbol{\sigma}$ denote the vectors containing the degrees of freedom of q_h, p_h , and $\boldsymbol{\sigma}_h$. By using the test function $w_h = \psi_j$ and the expansions $\boldsymbol{\sigma}_h = \sum_{i=1}^{N_V} \sigma_i(t) \psi_i(\mathbf{x})$ and $q_h = \sum_{i=1}^{N_W} q_i(t) \phi_i(\mathbf{x})$ in (3.15c), it follows that

$$\sum_{i=1}^{N_V} \left(\frac{1}{c(\boldsymbol{\mu})^2} \boldsymbol{\psi}_i, \boldsymbol{\psi}_j \right)_{\Omega_h} \sigma_i = - \sum_{i=1}^{N_W} (\phi_i, \nabla \cdot \boldsymbol{\psi}_j)_{\Omega_h} q_i.$$

The above equation can be converted to the matrix-vector form

$$\mathbf{M}_V(\boldsymbol{\mu})\boldsymbol{\sigma} = -\mathbf{S}\mathbf{q}, \quad (\text{C.1})$$

where the matrices $\mathbf{M}_V(\boldsymbol{\mu}) \in \mathbb{R}^{N_V \times N_V}$ and $\mathbf{S} \in \mathbb{R}^{N_V \times N_W}$ have components

$$(\mathbf{M}_V(\boldsymbol{\mu}))_{ij} = (c(\boldsymbol{\mu})^{-2}\boldsymbol{\psi}_i, \boldsymbol{\psi}_j)_{\Omega_h} = \sum_{k=1}^p \frac{1}{\mu_k^2} (\boldsymbol{\psi}_i, \boldsymbol{\psi}_j)_{\Omega_k} \quad (\mathbf{S})_{ji} = (\phi_i, \nabla \cdot \boldsymbol{\psi}_j)_{\Omega_h}.$$

Note that matrix $\mathbf{M}_V(\boldsymbol{\mu})$ depends affinely on $\boldsymbol{\mu}$ with coefficients $\boldsymbol{\mu}' = [\mu_1^{-2} \cdots \mu_p^{-2}]^\top$. Hence, $\mathbf{M}_V(\boldsymbol{\mu}) = \mathbf{T}\boldsymbol{\mu}'$ for the constant tensor $\mathbf{T} \in \mathbb{R}^{N_V \times N_V \times p}$ with entries $T_{ijk} = (\boldsymbol{\psi}_i, \boldsymbol{\psi}_j)_{\Omega_k}$. On the other hand, inserting the expansion $p_h = \sum_{i=1}^{N_W} p_i(t)\phi_i(\mathbf{x})$ and the above expansion for $\boldsymbol{\sigma}_h$ into (3.15b) and testing against $w_h = \phi_j$ yields

$$(\mathbf{M}_W \dot{\mathbf{p}})_j = \sum_{i=1}^{N_W} (\phi_i, \phi_j)_{\Omega_h} \dot{p}_i = \sum_{i=1}^{N_V} (\nabla \cdot \boldsymbol{\psi}_i, \phi_j)_{\Omega_h} \sigma_i = (\mathbf{S}^\top \boldsymbol{\sigma})_j.$$

By substituting for $\boldsymbol{\sigma}$ from (C.1), the equation can be written equivalently as

$$\mathbf{M}_W \dot{\mathbf{p}} = -\mathbf{S}^\top \mathbf{M}_V(\boldsymbol{\mu})^{-1} \mathbf{S} \mathbf{q} = -\mathbf{S}^\top (\mathbf{T}\boldsymbol{\mu}')^{-1} \mathbf{S} \mathbf{q}. \quad (\text{C.2})$$

Finally, using the test function $w_h = \phi_j$ and the above expansions of q_h and p_h , in (3.15a),

$$(\mathbf{M}_W \dot{\mathbf{q}})_j = \sum_{i=1}^{N_W} (\phi_i, \phi_j)_{\Omega_h} \dot{q}_i = \sum_{i=1}^{N_W} (\phi_i, \phi_j)_{\Omega_h} p_i = (\mathbf{M}_W \mathbf{p})_j. \quad (\text{C.3})$$

Together, (C.2) and (C.3) lead to the following block form of the FOM (3.15),

$$\dot{\mathbf{y}} = \begin{bmatrix} \dot{\mathbf{q}} \\ \dot{\mathbf{p}} \end{bmatrix} = \begin{bmatrix} \mathbf{0} & \mathbf{I} \\ -\mathbf{I} & \mathbf{0} \end{bmatrix} \begin{bmatrix} \mathbf{M}_W^{-1} \mathbf{S}^\top \mathbf{M}_V(\boldsymbol{\mu})^{-1} \mathbf{S} & \mathbf{0} \\ \mathbf{0} & \mathbf{I} \end{bmatrix} \begin{bmatrix} \mathbf{q} \\ \mathbf{p} \end{bmatrix}.$$

As a final point, the expression for the discrete Hamiltonian in (3.16) follows from (suppressing the dependence on $\boldsymbol{\mu}$)

$$\begin{aligned} H_h(q_h, p_h) &= \frac{1}{2} \left(\sum_{i=1}^{N_W} p_i \phi_i, \sum_{j=1}^{N_W} p_j \phi_j \right)_{\Omega_h} + \frac{1}{2} \left(\frac{1}{c^2(\cdot, \boldsymbol{\mu})} \sum_{i=1}^{N_V} \sigma_i \boldsymbol{\psi}_i, \sum_{j=1}^{N_V} \sigma_j \boldsymbol{\psi}_j \right)_{\Omega_h} \\ &= \frac{1}{2} \sum_{i=1}^{N_W} p_i \sum_{j=1}^{N_W} (\phi_i, \phi_j)_{\Omega_h} p_j + \frac{1}{2} \sum_{i=1}^{N_V} \sigma_i \sum_{j=1}^{N_V} \left(\frac{1}{c(\cdot, \boldsymbol{\mu})^2} \boldsymbol{\psi}_i, \boldsymbol{\psi}_j \right)_{\Omega_h} \sigma_j \\ &= \frac{1}{2} \sum_{i=1}^{N_W} \sum_{j=1}^{N_W} p_i (\mathbf{M}_W)_{ij} p_j + \frac{1}{2} \sum_{i=1}^{N_V} \sum_{j=1}^{N_V} \sigma_i (\mathbf{M}_V)_{ij} \sigma_j \\ &= \frac{1}{2} \mathbf{p}^\top \mathbf{M}_W \mathbf{p} + \frac{1}{2} \boldsymbol{\sigma}^\top \mathbf{M}_V \boldsymbol{\sigma} \\ &= \frac{1}{2} \mathbf{p}^\top \mathbf{M}_W \mathbf{p} + \frac{1}{2} (-\mathbf{M}_V^{-1} \mathbf{S} \mathbf{q})^\top \mathbf{M}_V (-\mathbf{M}_V^{-1} \mathbf{S} \mathbf{q}) \\ &= \frac{1}{2} \mathbf{p}^\top \mathbf{M}_W \mathbf{p} + \frac{1}{2} \mathbf{q}^\top \mathbf{S}^\top \mathbf{M}_V^{-1} \mathbf{S} \mathbf{q} \\ &= \frac{1}{2} \langle \mathbf{p}, \mathbf{p} \rangle_{\mathbf{M}_W} + \frac{1}{2} \langle \mathbf{q}, \mathbf{M}_W^{-1} \mathbf{S}^\top \mathbf{M}_V^{-1} \mathbf{S} \mathbf{q} \rangle_{\mathbf{M}_W}, \end{aligned}$$

where $\langle \mathbf{a}, \mathbf{b} \rangle_{\mathbf{M}_W} = \mathbf{a}^\top \mathbf{M}_W \mathbf{b}$ denotes the \mathbf{M}_W -weighted inner product.

References

- [1] B. M. AFKHAM AND J. S. HESTHAVEN, *Structure preserving model reduction of parametric Hamiltonian systems*, SIAM Journal on Scientific Computing, 39 (2017), pp. A2616–a2644, <https://doi.org/10.1137/17m1111991>.
- [2] J. BARNETT AND C. FARHAT, *Quadratic approximation manifold for mitigating the Kolmogorov barrier in nonlinear projection-based model order reduction*, Journal of Computational Physics, 464 (2022), p. 111348, <https://doi.org/10.1016/j.jcp.2022.111348>.
- [3] P. BENNER, S. GUGERCIN, AND K. WILLCOX, *A survey of projection-based model reduction methods for parametric dynamical systems*, SIAM Review, 57 (2015), pp. 483–531, <https://doi.org/10.1137/130932715>.
- [4] P. BENNER, M. OHLBERGER, A. PATERA, G. ROZZA, AND K. URBAN, *Model Reduction of Parametrized Systems*, vol. 17 of Modeling, Simulation and Applications, Springer International Publishing, 2017, <https://doi.org/10.1007/978-3-319-58786-8>.
- [5] G. BERKOOZ, P. HOLMES, AND J. LUMLEY, *The proper orthogonal decomposition in the analysis of turbulent flows*, Annual Review of Fluid Mechanics, 25 (1993), pp. 539–575, <https://doi.org/10.1146/annurev.fl.25.010193.002543>.
- [6] T. BERTALAN, F. DIETRICH, I. MEZIĆ, AND I. G. KEVREKIDIS, *On learning Hamiltonian systems from data*, Chaos: An Interdisciplinary Journal of Nonlinear Science, 29 (2019), p. 121107, <https://doi.org/10.1063/1.5128231>.
- [7] K. BHATTACHARYA, B. HOSSEINI, N. B. KOVACHKI, AND A. M. STUART, *Model reduction and neural networks for parametric PDEs*, The SMAI Journal of Computational Mathematics, 7 (2021), pp. 121–157, <https://doi.org/10.5802/smai-jcm.74>.
- [8] P. BUCHFINK, S. GLAS, AND B. HAASDONK, *Symplectic model reduction of Hamiltonian systems on nonlinear manifolds*. arXiv preprint, 2021, <https://arxiv.org/abs/2112.10815>.
- [9] J. DUAN AND J. S. HESTHAVEN, *Non-intrusive data-driven reduced-order modeling for time-dependent parametrized problems*, Journal of Computational Physics, 497 (2024), p. 112621, <https://doi.org/10.1016/j.jcp.2023.112621>.
- [10] I. FARCAS, R. GUNDEVIA, R. MUNIPALLI, AND K. E. WILLCOX, *Parametric non-intrusive reduced-order models via operator inference for large-scale rotating detonation engine simulations*, in AIAA SCITECH 2023 Forum, 2023, <https://doi.org/10.2514/6.2023-0172>.
- [11] N. R. FRANCO, A. MANZONI, AND P. ZUNINO, *A deep learning approach to reduced order modelling of parameter dependent partial differential equations*, Mathematics of Computation, 92 (2023), pp. 483–524, <https://doi.org/10.1090/mcom/3781>.
- [12] H. GAO, J.-X. WANG, AND M. J. ZAHR, *Non-intrusive model reduction of large-scale, nonlinear dynamical systems using deep learning*, Physica D: Nonlinear Phenomena, 412 (2020), p. 132614, <https://doi.org/10.1016/j.physd.2020.132614>.
- [13] R. GEELLEN, L. BALZANO, S. WRIGHT, AND K. WILLCOX, *Learning physics-based reduced-order models from data using nonlinear manifolds*, Chaos: An Interdisciplinary Journal of Nonlinear Science, 34 (2024), <https://doi.org/10.1063/5.0170105>.
- [14] R. GEELLEN, S. WRIGHT, AND K. WILLCOX, *Operator inference for non-intrusive model reduction with quadratic manifolds*, Computer Methods in Applied Mechanics and Engineering, 403 (2023), p. 115717, <https://doi.org/10.1016/j.cma.2022.115717>.
- [15] Y. GENG, L. JU, B. KRAMER, AND Z. WANG, *Data-driven reduced-order models for port-Hamiltonian systems with operator inference*. arXiv pre-print, 2025, <https://arxiv.org/abs/2501.02183>.

- [16] Y. GENG, J. SINGH, L. JU, B. KRAMER, AND Z. WANG, *Gradient preserving operator inference: Data-driven reduced-order models for equations with gradient structure*, *Computer Methods in Applied Mechanics and Engineering*, 427 (2024), p. 117033, <https://doi.org/10.1016/j.cma.2024.117033>.
- [17] O. GHATTAS AND K. WILLCOX, *Learning physics-based models from data: Perspectives from inverse problems and model reduction*, *Acta Numerica*, 30 (2021), p. 445–554, <https://doi.org/10.1017/s0962492921000064>.
- [18] W. R. GRAHAM, J. PERAIRE, AND K. Y. TANG, *Optimal control of vortex shedding using low-order models. Part I—Open-loop model development*, *International Journal for Numerical Methods in Engineering*, 44 (1999), pp. 945–972, [https://doi.org/10.1002/\(sici\)1097-0207\(19990310\)44:7%3c945::aid-nme537%3e3.0.co;2-f](https://doi.org/10.1002/(sici)1097-0207(19990310)44:7%3c945::aid-nme537%3e3.0.co;2-f).
- [19] M. GREPL AND A. PATERA, *A posteriori error bounds for reduced-basis approximations of parametrized parabolic partial differential equations*, *ESAIM: Mathematical Modelling and Numerical Analysis*, 39 (2005), pp. 157–181, <https://doi.org/10.1051/m2an:2005006>.
- [20] S. GREYDANUS, M. DZAMBA, AND J. YOSINSKI, *Hamiltonian neural networks*, *Advances in Neural Information Processing Systems*, 33 (2019), pp. 15379–15389, <https://dl.acm.org/doi/10.5555/3454287.3455665>.
- [21] A. GRUBER AND I. TEZAUR, *Canonical and noncanonical Hamiltonian operator inference*, *Computer Methods in Applied Mechanics and Engineering*, 416 (2023), p. 116334, <https://doi.org/10.1016/j.cma.2023.116334>.
- [22] A. GRUBER AND I. TEZAUR, *Variationally consistent Hamiltonian model reduction*, *SIAM Journal on Applied Dynamical Systems*, 24 (2025), pp. 376–414, <https://doi.org/10.1137/24m1652490>.
- [23] M. GUO AND J. S. HESTHAVEN, *Reduced order modeling for nonlinear structural analysis using Gaussian process regression*, *Computer Methods in Applied Mechanics and Engineering*, 341 (2018), pp. 807–826, <https://doi.org/10.1016/j.cma.2018.07.017>.
- [24] M. GUO AND J. S. HESTHAVEN, *Data-driven reduced order modeling for time-dependent problems*, *Computer Methods in Applied Mechanics and Engineering*, 345 (2019), pp. 75–99, <https://doi.org/10.1016/j.cma.2018.10.029>.
- [25] J. S. HESTHAVEN, C. PAGLIANTINI, AND N. RIPAMONTI, *Structure-preserving model order reduction of Hamiltonian systems*, in *Proceedings of the International Congress of Mathematicians*, vol. 7, 2022, pp. 5072–5097, <https://doi.org/10.4171/icm2022/100>.
- [26] Q. A. HUHN, M. E. TANO, J. C. RAGUSA, AND Y. CHOI, *Parametric dynamic mode decomposition for reduced order modeling*, *Journal of Computational Physics*, 475 (2023), p. 111852, <https://doi.org/10.1016/j.jcp.2022.111852>.
- [27] S. JAIN, P. TISO, J. B. RUTZMOSER, AND D. J. RIXEN, *A quadratic manifold for model order reduction of nonlinear structural dynamics*, *Computers & Structures*, 188 (2017), pp. 80–94, <https://doi.org/10.1016/j.compstruc.2017.04.005>.
- [28] P. JIN, Z. ZHANG, A. ZHU, Y. TANG, AND G. E. KARNIADAKIS, *SympNets: Intrinsic structure-preserving symplectic networks for identifying Hamiltonian systems*, *Neural Networks*, 132 (2020), pp. 166–179, <https://doi.org/10.1016/j.neunet.2020.08.017>.
- [29] D. E. KNUTH, *Two notes on notation*, *The American Mathematical Monthly*, 99 (1992), pp. 403–422, <http://www.jstor.org/stable/2325085> (accessed 2025-01-28).
- [30] B. KRAMER, B. PEHERSTORFER, AND K. E. WILLCOX, *Learning nonlinear reduced models from data with operator inference*, *Annual Review of Fluid Mechanics*, 56 (2024), pp. 521–548, <https://doi.org/10.1146/annurev-fluid-121021-025220>.

- [31] J. E. MARSDEN AND T. RATIU, *Introduction to Mechanics and Symmetry: A Basic Exposition of Classical Mechanical Systems*, Springer, 1998, <https://doi.org/10.1007/978-0-387-21792-5>.
- [32] S. A. MCQUARRIE, C. HUANG, AND K. E. WILLCOX, *Data-driven reduced-order models via regularised operator inference for a single-injector combustion process*, *Journal of the Royal Society of New Zealand*, 51 (2021), pp. 194–211, <https://doi.org/10.1080/03036758.2020.1863237>.
- [33] S. A. MCQUARRIE, P. KHODABAKHSHI, AND K. E. WILLCOX, *Non-intrusive reduced-order models for parametric partial differential equations via data-driven operator inference*, *SIAM Journal on Scientific Computing*, 45 (2023), pp. A1917–a1946, <https://doi.org/10.1137/21m1452810>.
- [34] B. PEHERSTORFER, *Sampling low-dimensional Markovian dynamics for preasymptotically recovering reduced models from data with operator inference*, *SIAM Journal on Scientific Computing*, 42 (2020), pp. A3489–a3515, <https://doi.org/10.1137/19m1292448>.
- [35] B. PEHERSTORFER AND K. WILLCOX, *Data-driven operator inference for nonintrusive projection-based model reduction*, *Computer Methods in Applied Mechanics and Engineering*, 306 (2016), pp. 196–215, <https://doi.org/10.1016/j.cma.2016.03.025>.
- [36] L. PENG AND K. MOHSENI, *Symplectic model reduction of Hamiltonian systems*, *SIAM Journal on Scientific Computing*, 38 (2016), pp. A1–a27, <https://doi.org/10.1137/140978922>.
- [37] E. QIAN, I.-G. FARCAŞ, AND K. WILLCOX, *Reduced operator inference for nonlinear partial differential equations*, *SIAM Journal on Scientific Computing*, 44 (2022), pp. A1934–a1959, <https://doi.org/10.1137/21m1393972>.
- [38] G. ROZZA, D. B. P. HUYNH, AND A. T. PATERA, *Reduced basis approximation and a posteriori error estimation for affinely parametrized elliptic coercive partial differential equations: Application to transport and continuum mechanics*, *Archives of Computational Methods in Engineering*, 15 (2008), pp. 229–275, <https://doi.org/10.1007/s11831-008-9019-9>.
- [39] T. SAYADI, P. J. SCHMID, F. RICHECOEUR, AND D. DUROX, *Parametrized data-driven decomposition for bifurcation analysis, with application to thermo-acoustically unstable systems*, *Physics of Fluids*, 27 (2015), <https://doi.org/10.1063/1.4913868>.
- [40] K. SCHÄCKE, *On the Kronecker product*, master’s thesis, University of Waterloo, 2004, <https://www.math.uwaterloo.ca/~hwolkowi/henry/reports/kronthesisschaecke04.pdf>.
- [41] P. J. SCHMID, *Dynamic mode decomposition of numerical and experimental data*, *Journal of Fluid Mechanics*, 656 (2010), p. 5–28, <https://doi.org/10.1017/s0022112010001217>.
- [42] P. J. SCHMID, *Dynamic mode decomposition and its variants*, *Annual Review of Fluid Mechanics*, 54 (2022), pp. 225–254, <https://doi.org/10.1146/annurev-fluid-030121-015835>.
- [43] P. SCHWERDTNER AND B. PEHERSTORFER, *Greedy construction of quadratic manifolds for nonlinear dimensionality reduction and nonlinear model reduction*. arXiv preprint, 2024, <https://arxiv.org/abs/2403.06732>.
- [44] H. SHARMA AND B. KRAMER, *Preserving Lagrangian structure in data-driven reduced-order modeling of large-scale dynamical systems*, *Physica D: Nonlinear Phenomena*, 462 (2024), p. 134128, <https://doi.org/10.1016/j.physd.2024.134128>.
- [45] H. SHARMA, H. MU, P. BUCHFINK, R. GEELEN, S. GLAS, AND B. KRAMER, *Symplectic model reduction of Hamiltonian systems using data-driven quadratic manifolds*, *Computer Methods in Applied Mechanics and Engineering*, 417 (2023), p. 116402, <https://doi.org/10.1016/j.cma.2023.116402>.
- [46] H. SHARMA, D. A. NAJERA-FLORES, M. D. TODD, AND B. KRAMER, *Lagrangian operator inference enhanced with structure-preserving machine learning for nonintrusive model reduction of mechanical systems*, *Computer Methods in Applied Mechanics and Engineering*, 423 (2024), p. 116865, <https://doi.org/10.1016/j.cma.2024.116865>.

- [47] H. SHARMA, Z. WANG, AND B. KRAMER, *Hamiltonian operator inference: Physics-preserving learning of reduced-order models for canonical Hamiltonian systems*, *Physica D: Nonlinear Phenomena*, 431 (2022), p. 133122, <https://doi.org/10.1016/j.physd.2021.133122>.
- [48] L. SIROVICH, *Turbulence and the dynamics of coherent structures. I. Coherent structures*, *Quarterly of Applied Mathematics*, 45 (1987), pp. 561–571, <https://doi.org/10.1090/qam/910462>.
- [49] M. A. SÁNCHEZ, B. COCKBURN, N.-C. NGUYEN, AND J. PERAIRE, *Symplectic Hamiltonian finite element methods for linear elastodynamics*, *Computer Methods in Applied Mechanics and Engineering*, 381 (2021), p. 113843, <https://doi.org/10.1016/j.cma.2021.113843>.
- [50] K. VEROY AND A. PATERA, *Certified real-time solution of the parametrized steady incompressible Navier-Stokes equations: Rigorous reduced-basis a posteriori error bounds*, *International Journal for Numerical Methods in Fluids*, 47 (2005), pp. 773–788, <https://doi.org/10.1002/flid.867>.
- [51] K. VEROY, C. PRUD'HOMME, D. ROVAS, AND A. PATERA, *A posteriori error bounds for reduced-basis approximation of parametrized noncoercive and nonlinear elliptic partial differential equations*, in *Proceedings of the 16th AIAA Computational Fluid Dynamics Conference*, Orlando, FL, 2003, <https://doi.org/10.2514/6.2003-3847>. Paper AIAA-2003-3847.
- [52] S. YUAN, *ODE-oriented semi-analytical methods*, in *Computational Mechanics in Structural Engineering*, F. Y. Cheng and Y. Gu, eds., Elsevier Science Ltd, Oxford, 1999, pp. 375–388, <https://doi.org/10.1016/b978-008043008-9/50067-3>.
- [53] S. YILDIZ, P. GOYAL, T. BENDOKAT, AND P. BENNER, *Data-driven identification of quadratic representations for nonlinear Hamiltonian systems using weakly symplectic liftings*, *Journal of Machine Learning for Modeling and Computing*, 5 (2024), pp. 45–71, <https://doi.org/10.1615/JMachLearnModelComput.2024052810>.
- [54] S. YILDIZ, P. GOYAL, P. BENNER, AND B. KARASÖZEN, *Learning reduced-order dynamics for parametrized shallow water equations from data*, *International Journal for Numerical Methods in Fluids*, 93 (2021), pp. 2803–2821, <https://doi.org/10.1002/flid.4998>.